IEEE Access
Multidisciplinary | Rapid Review | Open Access Journal

Received April 9, 2022, accepted April 26, 2022, date of publication May 3, 2022, date of current version May 11, 2022.

Digital Object Identifier 10.1109/ACCESS.2022.3172290

User-Centric Cell-Free and Co-Located Cellular Large Scale MU-MIMO Systems: A Comparative Performance Study With Spatial Channel Correlation in Dense Urban Scenario

AMR A. ALAMMARI, MOHD SHARIQUE, AND ATHAR ALI MOINUDDIN, (Member, IEEE)
Department of Electronics Engineering, Z. H. College of Engineering and Technology, Aligarh Muslim University, Aligarh 202002, India
Corresponding author: Amr A. Alammari (alammari.amr.rs@gmail.com)

ABSTRACT Large Scale Multi-user MIMO (LS-MU-MIMO) is a promising technology for the fifth-generation (5G) and beyond wireless systems. It offers several magnitudes of improvement in data rates and spectral efficiency (SE) due to its ability to suppress the interference and to have the properties of channel hardening and favourable propagation. In its conventional cellular paradigm, a large number of co-located antennas are deployed at the Base Station (BS) to serve a smaller number of user terminals (UTs). In order to deal with the inter-cell interferences more efficiently to achieve higher SE, a Cell-Free paradigm was proposed. Previous studies, which compare the two network deployments, relied on idealized assumptions, such as perfect channel state information, uncorrelated channels, and single-cell processing analysis-based, to name a few. This paper intends to bring further understanding of these two paradigms by examining the potential benefits of each paradigm in more realistic scenarios. Specifically, the influence of channel correlation on the achieved performance and network density in dense urban scenarios is investigated. Here, the performance of a Cell-Free network versus a traditional Co-located Cellular network structure has been compared in a more realistic setting. The comparison is carried out in different scenarios, taking into consideration the dense urban scenario, which supports low-to-moderate mobility and channel dispersion. First, we study the system performance gain in terms of Per-Terminal SE for different ratios of Antenna-UT and pilot scalers. Next, the Area-SE, defined as the sum SE of all UTs per unit area, is considered for different values of network density. Then, the channel estimation accuracy for both network deployments is compared, and its impact on the system performance as the Antenna-UT ratio increases is presented. Further, the impact of the spatially correlated channels is investigated in both network configurations. Finally, fronthaul requirements and distributed implementation in Cell-Free system deployment are discussed. Numerical simulations have been performed to investigate the performance gap between the two network deployments. Considering a cell-free system with scalable linear detectors and a large number of APs, the results show that the impact of noise and small-scale fading vanishes; moreover, a reduction in the non-coherent interference is observed in the same way as in the Co-located Cellular LS-MU-MIMO systems. The findings indicate that employing linear detectors results in non-increasing Per-Terminal SE as the network density increases. It is also found that Area-SE grows exponentially with the network density in both system deployments. Moreover, the increase in the Antenna-UT ratio improves the Per-Terminal SE and channel estimation accuracy. However, increasing the pilot scalers affects the systems' behavior in both deployments differently. Furthermore, local detection schemes are investigated, demonstrating the advantages of distributed implementation in the Cell-Free system in terms of reducing fronthaul signaling.

INDEX TERMS 5G, MU-MIMO, large scale MIMO, cell-free MIMO, spatial correlation channels, pilot contamination, channel estimation, LMMSE, area SE, local partial RZF.

The associate editor coordinating the review of this manuscript and approving it for publication was Stefan Schwarz.

I. INTRODUCTION

Fifth-generation (5G), also known as new radio, has been designed to cope with the constant increase in the demand for

higher rates of data services [1]. 5G systems are expected to provide ubiquitous connectivity and services to an unprecedented number of devices. The vision of 5G and beyond systems is to move the connections toward the recent realization of the Internet of Things (IoT), in which vehicles, sensors, robotic agents, home appliances, and wearable fitness and medical devices will interact with the end-users. Thus, it provides society with many game-changing services such as telesurgery, smart homes, self-driving cars, and advanced security systems [2]. To serve this massive number of devices, 5G and beyond networks have to increase the system capacity compared to the existing standards [3]. Large Scale Multi-user Multiple-input Multiple-output (LS-MU-MIMO) system, which deploys a large number of antennas at the base station (BS), is one among many promising key technologies for future cellular networks [4], [5]. Cellular LS-MU-MIMO communication systems are being deployed in recent 5G networks due to their ability to provide a significant improvement in the throughput and a great enhancement in the reliability, speed, and spectral efficiency [6]. Serving BSs with 64 antenna elements are available and have been in use since 2018 [7]. The idea behind this technology is to equip the BSs with a number of antennas much larger than the number of active user terminals (UT) per time and frequency resource. As a result, LS-MU-MIMO systems perform a coherent transmission that provides the system with unprecedented spatial resolution, array gains, and a reduction in interference, thus guaranteeing an increase in spectral efficiency (SE).

Antenna arrays at the BS in LS-MU-MIMO systems can be deployed in two different setups: Co-located or Distributed. In the Co-located cellular topology, all the antennas are located in a compact array at the BS, and each BS serves a specific group of UTs. In this network topology, the system performance can be improved by reducing the sizes of the cells in the network and applying proper signal processing and power control [8]. On the other hand, in the cellular distributed LS-MU-MIMO systems, the antennas are spread out over the coverage area. As a result, the system can provide a higher probability of coverage compared to the co-located LS-MU-MIMO. However, when it comes to the backhaul requirements, the co-located systems have the advantage of lower backhaul signaling compared to the distributed systems [9]. Modern signal processing techniques can be individually used in the BS to suppress the two types of interference (intra-cell and inter-cell interferences) without any cooperation between the BSs. However, in high-density networks, the performance of those systems still faces a limitation due to the interference from adjacent cells and large SNR variations, especially for the cell-edge UTs, which suffer more performance degradation [10]. Hence, 5G and beyond networks are expected to provide a better system performance in terms of uniform spectral efficiency and coverage. Many techniques have been proposed to tackle the performance degradation and solve the UTs location-related issues in the Cellular systems. For instance, to maintain a uniform service for all UTs, the concept of the distributed antenna system (DAS) was proposed to reduce the access distance [11], [12]. In the DAS-based structure, the antenna modules are distributed within each cell and connected to the home BS via wires, high-speed fiber optics, or RF links. Hence, the UTs close to the cell edge can be covered, and their performance improved. The coordinated multi-point (CoMP) is another concept to enhance the cell edge users' performance [13]. The idea is to evolve the existing cellular systems by allowing cooperation among the neighboring cells. Therefore, the cell edge user data rate and spectral efficiency can be improved with the cost of higher computational complexity and fronthaul signaling. The network can be divided into static disjoint cooperating clusters containing a few neighboring cells to reduce the computational complexity and the fronthaul signaling. Nevertheless, by dividing the network into disjoint cooperating clusters, residual inter-cluster interference still limits the system performance [14].

An alternative to the distributed LS-MU-MIMO systems is to deploy a cellular network with a large number of small cells. Each cell has a small, low-cost, and low-power BS serving only one UT [15]. This uncoordinated Small-Cell structure can mitigate the performance variations between the center and edge UTs. However, the system still suffers inter-cell interference due to its cell-centric structure.

From the above discussion, it can be concluded that inter-cell interference is unavoidable, and it is a fundamental limitation under the Cellular paradigm. Hence, there has been a great interest in shifting to a new network paradigm known as Cell-Free to overcome inter-cell interference and the performance degradation at the cell-edge UTs. This recently evolving concept uses LS-MU-MIMO, CoMP, and DAS technologies to produce a new network infrastructure called Cell-Free LS-MU-MIMO [16]. The Large-Scale term indicates that the cell-free structure employs a large number of access points (APs) spread out in the service area. Hence, the main idea is to install many Access Points (APs) across the area of coverage to serve the UTs via time division duplex (TDD) operation. Hence, each UT is being cooperatively served by a preferred set of surrounding APs. Similar to cellular distributed LS-MU-MIMO, the idea of having a large number of antenna elements to serve a smaller number of UTs is adopted in Cell-Free systems. Therefore, Cell-free LS-MU-MIMO is actually a specific realization of distributed LS-MU-MIMO with a user-centric structure. Compared to the conventional uncoordinated small cell system, where a UT is being served only by the closest antenna, Cell-Free can potentially provide better system performance [17]. To coordinate and process the transmission of all UTs in a Cell-Free system, all the APs are connected to a central processing unit (CPU) through fronthaul links. Thus, this network structure removes the cell boundaries and their corresponding inter-cell interference [18]. This paper aims to model and analyze such a user-centric system and evaluate the gain in the performance compared to a co-located cell-centric system.

Note that the transmitter in Cell-Free system is known as Access Point (AP), in Co-located Cellular and Small Cell

system architecture as Base station (BS), and in Distributed antenna systems as Remote Radio Heads (RRHs). Since Cell-Free (used here for user-centric) refers to a distributed network topology with no cell boundaries, the term Co-Cellular will be used to refer to the conventional Co-located Cellular LS-MU-MIMO systems in the remainder of this paper.

A. RELATED WORK

Conventional LS-MU-MIMO cellular networks have been studied extensively in many prior works [19]–[32]. To make the analysis tractable, most of the works consider three simplifying assumptions: i) the channel state information (CSI) is perfectly known at the BS (i.e., perfect CSI). However, this is not the case in practical scenarios where the channels have to be estimated at the receiver (i.e., imperfect CSI). The effect of perfect and imperfect CSI is investigated in [21], [22]; ii) the propagation channels between the UTs and the BSs are spatially uncorrelated [23], while practical channels are spatially correlated. Due to the lack of enough physical space to separate a large number of antennas in the BS, antenna correlation is inherent to the realization of Co-located LS-MU-MIMO systems. The effect of the channel correlation in multi-antenna systems with a large number of Co-located antennas was studied in [24]–[28]; iii) signal processing schemes designed for single-cell scenarios were applied, whereas multi-cell signal processing schemes can achieve better system performance [29]–[32]. For instance, a multi-cell Minimum Mean-Squared Error (MC-MMSE) detector that utilizes all the channel directions to suppress both intra-and-inter cell interferences is proposed in [30]. The authors have compared the proposed scheme with the single-cell scheme and shown that significant SE gains can be obtained. The performance analysis of cellular Co-located and distributed LS-MU-MIMO network setups has been studied and compared in [9], [33]–[35]. Results show that the distributed layout can achieve better performance and substantial data rate gains than the Co-located layout. Co-located LS-MU-MIMO architecture has the advantage of low backhaul signaling, thanks to the compact layout of the BS antennas. However, the distributed LS-MU-MIMO provides higher diversity gain and probability of coverage at the cost of increased backhaul signaling.

Recently, Cell-Free LS-MU-MIMO systems have gained considerable attention, and many papers in the literature have studied their performance from different perspectives [36]–[44]. For example, achievable spectral efficiency is derived for Maximum Ratio (MR) combining and conjugate beamforming (CB) in [38]. In [39] and [41], a stochastic geometry approach has been used to analyze the favorable propagation, channel hardening, and overall system performance. In [42], the system behavior was investigated over spatially correlated Rician fading. Further, a Cell-Free LS-MU-MIMO system with precoding and power optimization to maximize the data rate has been studied [43], [44]. The traditional Cell-Free deployment was originally developed under two original assumptions.

First, all the APs simultaneously serve all the active UTs in the system [41], [45], [46]. This assumption will result in making the framework unscalable in practice, which means that the system will not be able to handle a growing number of APs and UTs. To overcome this limitation and preserve the scalability, the key properties of the conventional LS-MU-MIMO systems and the user-centric architecture have been explored in [47]–[53]. A survey on user-centric cell-free massive MIMO systems with a comprehensive list of references to understand the cell-free systems has been recently published [49]. In the user-centric approach, each UT can select its set of serving APs from the neighborhood, which can be achieved by a clustering scheme known as dynamic cooperation clustering (DCC) [51], [53]. In the DCC scheme, each UT will be served by a subset of APs, and the scalability comes from decentralizing some signal processing between the APs and the CPU.

Second, the traditional Cell-Free deployment also assumed infinite fronthaul connections [44], [54]–[56]. However, when dealing with practical systems, each fronthaul link will have a limited capacity. Also, there is a need to limit the fronthaul signaling between the APs and the CPU to achieve scalability [49]. The performance of limited-fronthaul cell-free LS-MU-MIMO has been investigated in [36], [57], and [58].

Generally, there are two types of implementations in Cell-Free systems: fully centralized and distributed. In the fully centralized implementation, all the network processing is done at the CPU. The pilots and data signals are forwarded to the CPU, which will perform the required signal processing. However, when a large number of APs are installed in the coverage area, the burden on the fronthaul links is increased. The centralized implementation of Cell-Free deployments, where the channel estimation and data detection are accomplished at the CPU, is discussed in [59]–[61]. Taking the practical constraints of limited fronthaul capacity, this implementation will result in an overall unmanageable fronthaul signaling [62]. The decentralization in Cell-Free LS-MU-MIMO can be implemented in different levels, depending on how the signal processing is divided between the APs and the CPU. By distributing the network tasks between the CPU and the APs, the computational complexity will be less, and the overhead will be finite even with an increasing number of UTs. To reduce the fronthaul traffic, distributed operations are considered [61], [63]. In this distributed method, the required signal processing is done at the APs. The distributed implementation can be broadly distinguished from the centralized implementation in terms of three operations:

1) uplink channel estimates are computed locally at all APs; 2) combiners to be used at the APs are computed locally at each AP, and local data estimation is performed; 3) the fronthaul is used to send the local data estimates to the CPU and not for the channel estimates or the combiners.

When comparing the Cell-Free system with the previous systems, most of the studies focus on comparing it with the small cell counterpart [38], [39], [44], [64], where the system consists of a large number of distributed APs with

no cooperation between them. For example, authors in [38] analyzed the cell-free performance, taking into account the orthogonality of pilot sequences and the effect of channel estimation, and compared it with small cell systems. The results reveal that the Cell-Free deployment can provide a substantial improvement in the SE compared to the small cell deployment. In small cell systems, the CPU and the APs are limited to exchanging data and power control signals. Hence, it is clear that the Cell-Free LS-MU-MIMO systems outperform the small cell systems [65]. Therefore, to quantify the gain in the performance, it is better to compare the Cell-Free system to the conventional Co-Cellular system.

Further, the performance analysis discussed in the literature is mostly based on linear MR or Zero Forcing (ZF) combining schemes; for example, [44], [66], and [67]. However, there is a need to evaluate the system performance with more advanced combining schemes like Regularized Zero-Forcing (RZF) and MMSE, which have already been proposed for the conventional LS-MU-MIMO systems [30].

This paper is an attempt to address the above points. First, we consider the centralized implementation to investigate its ability of interference cancellation. Then, the local distributed operations with different combining schemes have been studied. It is assumed that the channels have to be estimated in a training phase, in which a Bayesian Linear MMSE (LMMSE) channel estimator is employed. The performance in the uplink of Cell-Free deployment is studied and compared with Co-Cellular LS-MU-MIMO deployment to analyze the impact of no-cell structure on the achievable sum rate. The effects of channel correlation, pilot contamination, pilot scaling, and the Antenna-UT ratio are taken into consideration for more realistic system deployment scenarios. Moreover, this work investigates the impact of AP/BS densification on the uplink per-terminal SE of both system deployments by introducing the concept of network density. (see [28], [68]–[70] for more results on this concept in cellular systems.)

B. CONTRIBUTIONS OF THE PAPER

The existing literature contributions typically consider the traditional structure of Cell-Free LS-MU-MIMO system, in which all the APs serve all the active UTs in the network at the same time. However, this structure is both power inefficient and impractical because only a portion of the APs can beneficially transmit to a certain UT. A practical variant of Cell-Free system known as the user-centric architecture allows each UT to dynamically select its set of serving APs. Further, most of the works in the literature compare the traditional Cell-Free deployment with a variant of the Cellular system, i.e., small cell deployment, where a large number of uncooperative BSs serve only one UT.

Taking into account the aforementioned gap in the literature, this paper aims to reconsider the comparison between User-Centric Cell-Free and Co-Cellular system deployments under practical scenarios and realistic system specifications. The contribution of this paper can be summarized as follows:

- *System modeling*: In this work, we consider the uplink of a LS-MU-MIMO system with finite capacity fronthaul links. To capture the impact of no-cell structure on the achieved performance, we present a point-to-point comparison between user-centric Cell-Free and conventional Co-Cellular system architectures. The two system deployments are mathematically modeled and numerically simulated. The objective of this study is to give a further understanding and a comprehensive comparison of both system deployments under more realistic and practical system considerations. Unlike previous works, and to maintain fairness in the comparison, we provide unified settings that can be applied for both system deployments to preserve the same network density (i.e., the same number of antenna elements and the same number of UTs).
- *Physical layer signal processing*: We identify the main physical layer operations in the deployment of LS-MU-MIMO uplink transmission, including uplink signaling, CSI estimation, data detection, and fronthaul signaling. In continuity with previous works, this paper focuses on the case of sub-6 GHz carrier frequencies, leaving higher frequencies for future research.
- *Performance analysis*: Under spatially correlated channels and imperfect CSI, we quantitatively evaluate the User-Centric Cell-Free system's performance in comparison to that of Co-Cellular systems. We analyze the SE and Area-SE (ASE) performances of both network deployments for a dense urban scenario that can support low-to-moderate channel dispersion and mobility. This is a reasonable consideration in Cell-Free network deployments since the APs are deployed near the UTs. Simulation and numerical results are given for three Scalable linear detectors in Cell-Free: Partial MMSE (PMMSE), Partial RZF (PRZF), Centralized MR (MR-Cent.). They are also given for four linear detectors in Co-located Cellular: Multicell-MMSE (MC-MMSE), Single-cell MMSE (SC-MMSE), single-cell RZF (SC-RZF), and MR. This allows us to get insights into the system performance and investigate the system behaviour with different scenarios, i.e., network density, pilot scaling factor, and the ratio of Antenna-UT.
- *Analysis of two Cell-Free implementations:* Based on the above analysis, we adopt three Cell-Free system implementations, namely, fully centralized, local distributed, and two-stage local distributed. We study how competitive the local distributed-based combining schemes are to centralized-based schemes in spectral efficiency and overall system performance. Extensive simulation results evaluate the system's achieved SE performance of the three implementations from different aspects (e.g., the impact of scaling the pilot length and the number of deployed APs) and for different combining schemes: PRZF, Local PRZF (LPRZF), and distributed MR (MR-Dist.).

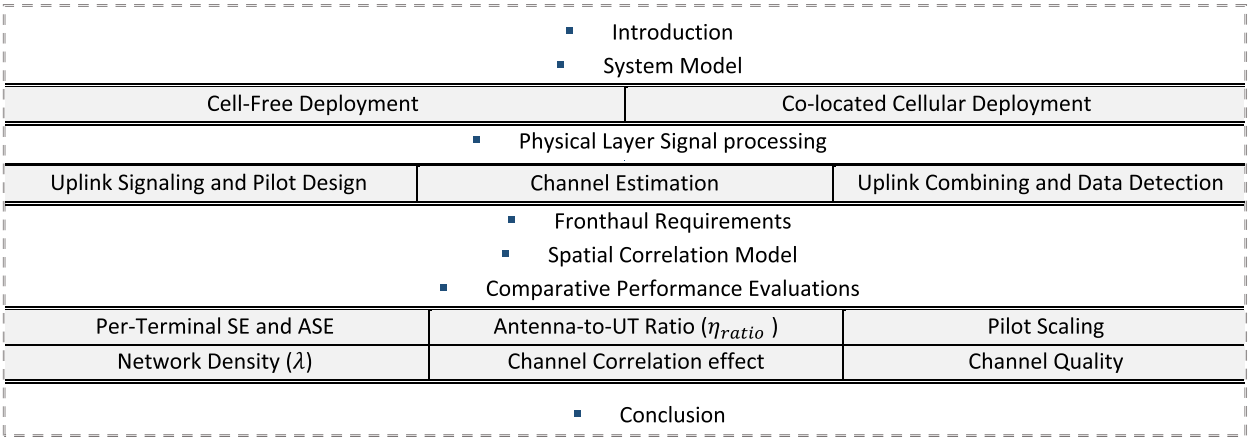

FIGURE 1. Paper structure.

TABLE 1. Notations and symbols.

Notation	Definition
$(\cdot)^{\mathrm{H}}$	Hermitian transpose
$\mathrm{tr}(\cdot)$	Trace operator
$\mathbb{E}\{\cdot\}$	Expectation value
$\|\cdot\|$	Euclidean norm
$dig(\mathbf{A},\ldots,\mathbf{A}_{\mathrm{n}})$	Block-diagonal matrix
$\mathcal{N}_C\left(0,\sigma\right)$	Zero-mean circularly symmetric complex Gaussian random vector with standard deviation σ
Symbol	**Definition**
η_{ratio}	Antenna-UT Ratio
ζ	Pilot Scaling Factor
β	Average gain
λ	Network Density
$\overline{MSE}$	Normalized Minimum Square Error

C. PAPER ORGANIZATION AND NOTATION

The paper structure is illustrated in Fig. 1, and the rest of this paper is organized as follows: The LS-MU-MIMO system model for both network deployments is described in section II. Section III presents the signal processing in Cell-Free and Co-located Cellular physical layer. The fronthaul requirements and the channel model considered in this work are presented in sections IV and V, respectively. The simulation results and the discussion are presented in section VI, followed by the conclusion in section VII. This paper uses the notions and symbols listed in table 1.

II. SYSTEM DESCRIPTION

This section introduces the uplink transmission scenario in two Cell-Free and Co-located Cellular deployments of LS-MU-MIMO. A large number of single-antenna APs distributed in a large geographic area are considered in the former, and a few BSs deployed with a large number of co-located antennas are considered in the latter. Fig. 2 shows the system deployment in both scenarios. The two networks operate in a TDD mode, where each AP (or BS) estimates the uplink channels from UTs depending on their transmitted uplink pilots. Due to the reciprocity in the TDD mode, these estimates can also be used for the downlink channels.

For both network deployments considered in this work, we use the following definitions in the system model description:

Definition 1: In a given geographical area, a cell-Free LS-MU-MIMO system consists of:

- A large number of single-antenna APs;
- More APs than active users: $L \gg K$ or $\frac{L}{K} > 1$;
- All APs connected to one CPU.

Definition 2: In a given limited area, a Co-Cellular LS-MU-MIMO system consists of:

- $N \geq 2$ cells, each cell has a single BS;
- $M \geq 64$ antenna in each BS;
- $K \geq 8$ active user terminals (UTs) per cell and overall $M \gg K$ or $\frac{\mathrm{M}}{\mathrm{K}} > 1$.

We assume that the APs in the Cell-Free and the BSs in the Co-Cellular LS-MU-MIMO are deployed in a dense urban scenario and consider all its propagation conditions. Further, the channels in the two deployments are modeled as block fading, where the channels are constant and frequency flat in one coherence block and changes between blocks. In each coherence block, the channel takes one independent realization. The length of this coherence block depends on many factors: carrier frequency, mobility, the propagation environment, etc. In the block fading model, each coherence block consists of τ_{c} complex-valued samples used for uplink pilot training $\left(\tau_{\mathrm{p}}\right)$, uplink data transmission(τ_{u}), and downlink data transmission (τ_{d}). The channel model includes two main effects: small-scale fading and large-scale fading, where the small-scale fading is assumed to be constant in one coherence block and independently changes between the consecutive blocks.

The large-scale fading changes slower than the small-scale fading and can be static for several coherence blocks. The channel responses between the l^{th} AP (or the *mth* BS's antenna), and the k^{th}UT is assumed to have a correlated

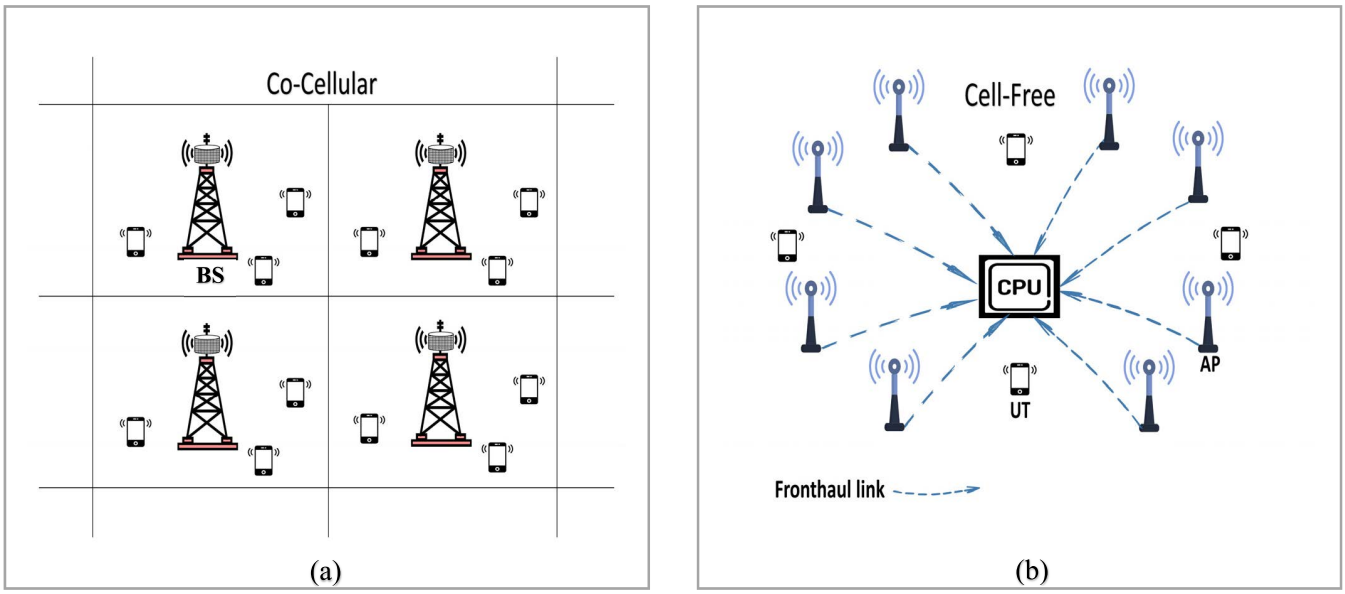

FIGURE 2. Comparison between '(a) Co-located cellular and (b) cell free' large scale MU-MIMO systems.

rayleigh fading distribution, which can be modeled as,

$$\mathbf{h}_{\mathcal{X}} \sim \mathcal{N}_C\left(0, \mathbf{R}_{\mathcal{X}}\right). \tag{1}$$

where the two fading effects are composed in the spatial correlation matrix $\mathbf{R}_{\mathcal{X}}$ and the indices of $\mathbf{h}$ and $\mathbf{R}$ follow the corresponding system deployment.

A. CELL-FREE DEPLOYMENT

Consider a multi-user Cell-Free system with L single-antenna APs randomly distributed in the area of coverage and simultaneously serving K single-antenna UTs, which are also randomly located in the area. The UT k in the cell-free deployment is served by a group of APs, i.e., the set $\mathcal{Q}_k \subset \{1, 2, \ldots\ldots, L\}$, which is the set of APs that cooperate to serve the UT k. As illustrated in Fig. 2 (b), all the APs in the Cell-Free (CF) system are connected to a central processing unit (CPU) through fronthaul links. The CPU collects the pilots and the transmitted data received at all APs to perform channel estimation and data detection.

Let x_i be the transmitted signal from the UT i to the AP l and the corresponding superposition of the received signals at the AP l denoted by $\boldsymbol{y}_l^{CF}$ and given by [71]

$$\boldsymbol{y}_l^{CF} = \sqrt{p}_u \sum_{i=1}^{K} \boldsymbol{h}_{il} x_i + \boldsymbol{w}_l. \tag{2}$$

where p_u denotes the average uplink power transmitted by UTs, and $\boldsymbol{w}_l$ denotes the additive independent receiver noise, which is modeled as $\boldsymbol{w}_{\text{noise}} \sim \mathcal{N}_C\left(0, \sigma^2\right)$.

In the Cell-Free deployment, each user is being served by a sub-group of APs. Hence, the operations performed by the CPU have to deal with all the transmitted signals received by the same group of APs.

Let $\boldsymbol{y}_{cpu}^{CF}$ denotes the collective transmitted signals received by all APs, which is related to UT i and given by

$$\begin{aligned} \boldsymbol{y}_{cpu}^{CF} &= \left[\boldsymbol{y}_1^{CF}, \boldsymbol{y}_2^{CF}, \ldots\ldots, \boldsymbol{y}_L^{CF}\right]^T \\ &= \sum_{i=1}^{K} \boldsymbol{h}_i x_i + \boldsymbol{w}. \end{aligned} \tag{3}$$

where $\boldsymbol{w}$ is a vector that includes all the received noise in all APs, which is related to the UT i, i.e.,

$$\boldsymbol{w} = \left[\boldsymbol{w}_1^T, \boldsymbol{w}_2^T, \ldots\ldots, \boldsymbol{w}_L^T\right]^{\mathrm{T}}. \tag{4}$$

Suppose, for now, that the channel statistics are known at the network. Hence, to detect the transmitted signal x_i, the CPU has to select an appropriate receive combiner to separate the desired transmitted signal from the interference and noise. Let $\mathbf{a}_k^{\mathrm{H}}\mathbf{D}_k$ be the vector used to find the estimate of the received signal x_i, where $\mathbf{a}_k^{\mathrm{H}}$ is the receive combining vector, and $\mathbf{D}_k$ is a block diagonal matrix introduced to ensure that only the APs serving UT k will be involved in the signal detection process. Simply stated, $\mathbf{D}_k$ is the identity matrix if the AP belongs to the set of APs that serve the UT k and are allowed to take part in the signal detection at the CPU and zero otherwise. Hence, the estimate of the transmitted signal at the CPU can be written as,

$$\begin{aligned} \hat{x}_k &= \boldsymbol{a}_k^H \boldsymbol{D}_k \boldsymbol{y}_{cpu}^{CF}. \\ &= \boldsymbol{a}_k^H \boldsymbol{D}_k \boldsymbol{h}_k x_k + \sum_{\substack{i=1 \\ i \neq k}}^{K} \boldsymbol{a}_k^H \boldsymbol{D}_k \boldsymbol{h}_i x_i + \boldsymbol{a}_k^H \boldsymbol{D}_k \boldsymbol{w}. \end{aligned} \tag{5}$$

where the first term represents the desired transmitted signal, the second represents the interference from other users, and the third term is the noise.

B. CO-CELLULAR DEPLOYMENT

This section describes the Co-Cellular system deployment for comparative study with respect to the Cell-Free system deployment presented in section A. In the conventional

Co-Cellular LS-MU-MIMO system, the UT can only be served by one BS at a time (except during handover). Consider a multi-cellular network with N cells; each cell has a single BS equipped with M array antennas, communicating simultaneously with single-antenna K UTs. In the Co-Cellular deployment (Co-Cell), the BS j receives signals from UTs in the uplink scenario and is commonly expressed as [72]

$$\boldsymbol{y}_j^{Co-Cell} = \sqrt{p}_u \sum_{n=1}^{N} \sum_{k=1}^{K_n} \boldsymbol{h}_{nk}^{j} x_{nk} + \boldsymbol{w}_j. \tag{6}$$

where p_u and $\boldsymbol{w}_j$ are defined in the same way as in (2). Also, similar to (5), the estimated transmitted signal at BS j can be detected by selecting a receive combiner $\boldsymbol{a}_k^{\mathrm{H}}$ to separate the desired signal from the interference and noise. Analytically, it can be expressed as

$$\begin{aligned}\hat{x}_k &= \boldsymbol{a}_{jk}^{H} \boldsymbol{y}_j^{Co-Cell}. \\ &= \sqrt{p}_u \sum_{n=1}^{N} \sum_{k=1}^{K_n} \boldsymbol{a}_{jk}^{H} \boldsymbol{h}_{nk}^{j} x_{nk} + \boldsymbol{a}_{jk}^{H} \boldsymbol{w}_j. \\ &= \sqrt{p}_u \boldsymbol{a}_{jk}^{H} \boldsymbol{h}_{jk}^{j} x_{jk} + \sqrt{p}_u \sum_{\substack{i=1 \\ i \neq k}}^{K} \boldsymbol{a}_{jk}^{H} \boldsymbol{h}_{ji}^{j} x_{ji} \\ &\quad + \sqrt{p}_u \sum_{\substack{n=1 \\ n \neq j}}^{N} \sum_{i=1}^{K_n} \boldsymbol{a}_{jk}^{H} \boldsymbol{h}_{ni}^{j} x_{ni} + \boldsymbol{a}_{jk}^{H} \boldsymbol{w}_j. \end{aligned} \tag{7}$$

where the first term represents the desired transmitted signal, the second and third terms represent the interference from the user's own cell and the interference from different cells respectively, and the fourth term is the noise. As can be seen from (7), and in contrast to Cell-Free, all BSs in the Co-Cellular system are involved in the signal processing.

III. PHYSICAL LAYER SIGNAL PROCESSING

This section presents the main signal processing operations for LS-MU-MIMO systems for comparative performance evaluation of the considered network deployments. In the LS-MU-MIMO uplink transmission, these operations include uplink signaling, channel estimation, and data detection as the main physical layer processing operations.

A. UPLINK TRAINING

In the uplink training phase, a similar training process takes place between the UTs and the APs in both system deployments. The UTs send training symbols known as pilot symbols to the APs (or BSs in the case of Co-Cellular). The pilot sequence is assumed to be of length τ_p for each user. Also, there are τ_p orthogonal pilot sequences available in the network, i.e., we have $\boldsymbol{\Psi} = \left[\boldsymbol{\psi}_1, \boldsymbol{\psi}_2, \ldots\ldots, \boldsymbol{\psi}_{\tau_p}\right]$ orthogonal pilot sequences. However, the number of UTs is assumed to be larger than the available orthogonal pilot sequences ($K > \tau_p$), leading to the reuse of the same pilot sequences by more than one UT. The sharing of the same pilot sequences is the reason behind a well-known problem in the LS-MU-MIMO systems called pilot contamination.

In the Cell-Free LS-MU-MIMO, let $\mathbf{Y}_l^{pilot}$ be the matrix of the received pilot training signals at the AP l and can be written as

$$\mathbf{Y}_l^{pilot} = \sqrt{p}_p \sum_{i=1}^{K} \boldsymbol{h}_{il} \boldsymbol{\psi}_{t_i}^{H} + \boldsymbol{W}_l. \tag{8}$$

where p_p denotes the power of the transmitted pilot, $\boldsymbol{\psi}_{t_i}^{H}$ is the pilot sequence transmitted by the ith UT, and $\boldsymbol{W}_l$ denotes the additive white Gaussian noise, which is i.i.d with zero mean and unity variance. The received signal $\mathbf{Y}_l^{pilot}$ correlated with $\boldsymbol{\psi}_{t_k}^{*}$, which is the conjugate of the pilot sequence of thei^{th} UT, leading to $\mathbf{y}_{t_k l}^{pilot}$, given as

$$\begin{aligned}\mathbf{y}_{t_k l}^{pilot} &= \mathbf{Y}_l^{pilot} \boldsymbol{\psi}_{t_k}^{*} \\ &= \sum_{i=1}^{K} \boldsymbol{h}_{il} \boldsymbol{\psi}_{t_i}^{H} \boldsymbol{\psi}_{t_k}^{*} + \boldsymbol{W}_l \boldsymbol{\psi}_{t_k}^{*}. \end{aligned} \tag{9}$$

In the Co-Cellular system deployment, the received pilot signal can be generated in the same way as in (9). Hence, the processed received pilot signal for both system deployments can be further normalized and simplified as follows,

$$\begin{aligned}&\mathbf{y}_{t_k l/j}^{\text{pilot}} \\ &= DS + UI + W \\ &= \begin{cases} \sqrt{p_p \tau_p} \boldsymbol{h}_{kl} + \sum_{i \in \wp_k \setminus \{k\}} \sqrt{p_p \tau_p} \boldsymbol{h}_{il} + \boldsymbol{W}_l \boldsymbol{\psi}_{t_k}^{*}. \\ \quad CF \\ \sqrt{p}_p \tau_p \boldsymbol{h}_{jk}^{j} + \sum_{(n,i) \in \wp_k \setminus \{j,k\}} \sqrt{p}_p \tau_p \boldsymbol{h}_{ni}^{j} + \boldsymbol{W}_j \boldsymbol{\psi}_{t_k}^{*}. \\ \quad Co-Cell \end{cases} \end{aligned} \tag{10}$$

where the first term represents the desired pilot (DS), the second term is the interference from sharing the same pilot between UTs (UI), and the last denotes the noise (W). Note that $\wp_k$ is the set of UTs that share the same pilot sequence as UT k. The processed signal $\mathbf{y}_{t_k l/j}^{pilot}$ is the statistics that the CPU (in Cell-Free) and the BS (in Co-Cellular) use to estimate the channel.

B. LMMSE CHANNEL ESTIMATION

Since the channel statistics are not exactly known in practical scenarios, the received pilot signal $\mathbf{y}_{t_k l/j}^{pilot}$ in the Cell-Free and Co-Cellular systems are used to estimate the channels to UTs. The LMMSE estimator is employed in both deployments to estimate the channel coefficients between the UTs and the APs (or the BSs). For simplicity, let $\boldsymbol{h}_\chi$ denotes the channel to be estimated in both system deployments, where $\boldsymbol{h}_\chi = \boldsymbol{h}_{kl}$ in Cell-Free system and $\boldsymbol{h}_\chi = \boldsymbol{h}_{jk}$ in Co-Cellular system. Based on the estimation theory, the channel $\boldsymbol{h}_\chi$ between the UT k, and the AP (or the BS) can be expressed as [73]

$$\hat{\boldsymbol{h}}_\chi = \sqrt{p_p \tau_p} \mathbf{R}_\chi \mathbf{Q}_{corr} \mathbf{y}_{t_k l/j}^{pilot}. \tag{11}$$

where $\mathbf{R}_\chi$ is the spatial correlation matrix of the channel intended to be estimated, and $\mathbf{Q}_{\text{corr}}$ is the inverse of the normalized correlation matrix of $\mathbf{y}_{t_k l/j}^{pilot}$ and can be given as

$$\mathbf{Q}_{corr} = \mathbb{E}\left\{ \mathbf{y}_{t_k l/j}^{pilot} \left(\mathbf{y}_{t_k l/j}^{pilot} \right)^{H} \right\}$$

TABLE 2. Linear detectors to maximize the SINR in cell-free and co-cellular.

	Cell-Free	Co-Cellular
$\boldsymbol{a}^{MMSE}$	$p_k\left(\sum_{i\in\mathcal{S}_k} p_i \mathbf{D}_k \widehat{\boldsymbol{h}}_i \widehat{\boldsymbol{h}}_i^H \mathbf{D}_k + \sum_{i\in\mathcal{S}_k} p_i \mathbf{D}_k \mathbf{C}_{err} \mathbf{D}_k + \sigma^2 I_{\mathrm{L}}\right)^{-1} \mathbf{D}_k \widehat{\boldsymbol{h}}_k$	$p_{jk}\left(\sum_{n=1}^{N}\sum_{i=1}^{K_n} p_{ni}\left(\widehat{\boldsymbol{h}}_{ni}^{j}\right)\left(\widehat{\boldsymbol{h}}_{ni}^{j}\right)^H + \mathbf{C}_{err}\right) + \sigma_{UL}^2 I_{M_j}\Big)^{-1} \widehat{\boldsymbol{h}}_{jk}^{j}$
$\boldsymbol{a}^{RZF}$	$p_k\left(\sum_{i\in\mathcal{S}_k} p_i \mathbf{D}_k \widehat{\boldsymbol{h}}_i \widehat{\boldsymbol{h}}_i^H \mathbf{D}_k + \sigma^2 I_{\mathrm{L}}\right)^{-1} \mathbf{D}_k \widehat{\boldsymbol{h}}_k$	$p_{jk}\left(p_{jk}\widehat{\boldsymbol{h}}_{jk}^{j}\left(\widehat{\boldsymbol{h}}_{jk}^{j}\right)^H + \sigma_{UL}^2 I_{M_j}\right)^{-1} \widehat{\boldsymbol{h}}_{jk}^{j}$
$\boldsymbol{a}^{MR}$	$\mathbf{D}_k \widehat{\boldsymbol{h}}_k$	$\widehat{\boldsymbol{h}}_{jk}^{j}$

$$= \begin{cases} \left(\sum_{i\in\wp_k} p_p \tau_p \boldsymbol{R}_{il} + \sigma^2\right)^{-1} & CF \\ \left(\sum_{(n,i)\in\wp_k\setminus\{j,k\}} p_p \tau_p \boldsymbol{R}_{ni} + \sigma^2 I_{M_j}\right)^{-1} & Co\text{-}Cell \end{cases} \tag{12}$$

Note that the indices of $\mathbf{Q}_{\mathrm{corr}}$ will be the same as the indices of the corresponding processed received signal $\mathbf{y}_{t_k l/j}^{pilot}$ for both system deployments.

Let $\mathbf{e}_\chi = \boldsymbol{h}_\chi - \hat{\boldsymbol{h}}_\chi$ be the estimation error that occurs during the estimation process and the expectation $\mathbb{E}\left\{\left\|\boldsymbol{h}_\chi - \hat{\boldsymbol{h}}_\chi\right\|^2\right\}$ is the quality of the estimation process in the LMMSE estimator, which can be given by taking the trace of the correlation matrix of $\boldsymbol{e}_\chi$. In the LMMSE estimation process, both the estimation and the estimation error are statistically independent random variables. The covariance matrices of the channel estimate $\hat{\boldsymbol{h}}_\chi$ and the channel estimation error $\boldsymbol{e}_\chi$ for the two system deployments can be given as follows

$$\mathbf{C}_{\mathrm{est.}} = \mathbb{E}\left\{\hat{\boldsymbol{h}}_\chi \left(\hat{\boldsymbol{h}}_\chi\right)^{\mathrm{H}}\right\} = p_p \tau_{\mathrm{p}} \mathbf{R}_\chi \mathbf{Q}_{corr} \mathbf{y}_{t_k l/j}^{pilot} \mathbf{R}_\chi \tag{13}$$

$$\mathbf{C}_{\mathrm{err.}} = \mathbb{E}\left\{\boldsymbol{e}_\chi \left(\boldsymbol{e}_\chi\right)^{\mathrm{H}}\right\} = \mathbf{R}_\chi - p_p \tau_{\mathrm{p}} \mathbf{R}_\chi \mathbf{Q}_{corr} \mathbf{y}_{t_k l/j}^{pilot} \mathbf{R}_\chi \tag{14}$$

Finally, in the Cell-Free system and similar to the analysis in section II, the collective statistics of the channels from UT k to all corresponding APs have to be available for processing to estimate the channel at the CPU. Where $\mathbf{D}_k\hat{\boldsymbol{h}}_k = \left[\mathbf{D}_{k1}\hat{\boldsymbol{h}}_{k1} \ldots .., \mathbf{D}_{kL}\hat{\boldsymbol{h}}_{kL}\right]$ is the estimation of the channel $\boldsymbol{h}_k$ from UT k to all its serving APs ($\mathcal{Q}_k$). Consequently, the matrices $\mathbf{R}_k$, $\mathbf{Q}_{t_k l}$ and $\mathbf{C}_{\mathrm{err.}}$ are defined as *diag* $(\mathbf{R}_{k1}, \ldots, \mathbf{R}_{kL})$, *diag* $\left(\mathbf{Q}_{t_k 1}, \ldots, \mathbf{Q}_{t_k L}\right)$, and *diag* $(\mathbf{C}_{\mathrm{err.1}}, \ldots, \mathbf{C}_{\mathrm{err.L}})$, respectively.

C. UPLINK COMBINING AND DATA DETECTION

After the channels to the active UTs are estimated, the UTs send the uplink data signals. These uplink signals are received at the APs (or BSs) and processed to detect the transmitted signal $\hat{x}_k$ in the same way as in (5) and (7). Let DS denotes the desired signal, and UI denotes the multi-user interference, the estimated signal after applying the receive combining vector $\mathbf{a}_k^{\mathrm{H}}$ can be written as

$$\hat{x}_k = \mathbf{a}_k^{\mathrm{H}}\left(DS_{\mathrm{k}} + UI + \boldsymbol{w}\right) \tag{15}$$

where $\mathbf{a}_k^{\mathrm{H}}$ is defined similarly as in section II for Cell-Free and Co-Cellular systems, and DS_{k} is the desired received signal through the estimated and estimation error channels and can be expressed as

$$DS_{\mathrm{k}} = \mathbf{a}_k^{\mathrm{H}}\left(\hat{\boldsymbol{h}}_\chi + \boldsymbol{e}_\chi\right) x_k = \mathbf{a}_k^{\mathrm{H}}\hat{\boldsymbol{h}}_\chi x_k + \mathbf{a}_k^{\mathrm{H}}\boldsymbol{e}_\chi x_k \tag{16}$$

The interference from different users (UI) is given as

$$UI = \begin{cases} \sum_{\substack{i=1 \\ i\neq k}}^{K} \boldsymbol{a}_k^H \boldsymbol{D}_k \boldsymbol{h}_i x_i \\ CF \\ \sum_{\substack{i=1 \\ i\neq k}}^{K} \boldsymbol{a}_{jk}^H \boldsymbol{h}_{ji}^{j} x_{ji} + \sum_{\substack{n=1 \\ n\neq j}}^{N}\sum_{i=1}^{K_n} \boldsymbol{a}_{jk}^H \boldsymbol{h}_{ni}^{j} x_{ni} \\ Co\text{-}Cell \end{cases} \tag{17}$$

where in the Cell-Free system, the UI term contains interference from UTs communicating with a set of $\mathcal{Q}_k \subset \{1, 2, \ldots\ldots, L\}$ only. However, in the Co-Cellular system, the multi-user interference in (17) contains the interference from the cell's own users (first term) and interference from users in the different cells (second term).

Since the vector $\mathbf{a}_k^{\mathrm{H}}$ contains the combining vectors of all APs serving the desired UT k, the detection process in Cell-Free is limited to that group of APs (i.e., $\mathcal{Q}_k \subset \{1, 2, \ldots\ldots, L\}$), while the detection process in the Co- Cellular system involves all the BSs in the processing.

The exact expression of the ergodic capacity in LS-MU-MIMO system remains unknown. However, bounds on the ergodic capacity, also known as achievable spectral efficiency (SE), are available and can be used as a performance metric.

In this section, we employ an asymptotic lower bound to investigate the scaling behavior of the UT k average uplink capacity with Cell-Free and Co-Cellular system deployments.

The achievable SE of UT k is introduced in lemma 1.

Lemma 1: When using LMMSE channel estimation and linear processing, an achievable uplink SEs of Cell-Free and Co-located system deployments of UT k are given as (18) and (19), shown at the bottom of the next page, where SINR denotes the uplink signal to interference and noise ratio of UT k and is given by (20a) and (20b) (*shown at the bottom of the next page*) for Cell-Free deployment and Co-Cellular deployment, respectively.

Proof: The proof follows from the same procedure of lower-bounding adopted in [16] for Cell-free system deployment and [25] for the Co-Cellular system deployment. It is noteworthy that the expression in (18) and (19) can be computed using instantaneous Channel realizations. The ratio inside the logarithm in both expressions can be interpreted as the uplink effective instantaneous SINR because it includes both instantaneous estimated CSI and average over CSI estimation errors. Since this average over CSI estimation errors is not available instantaneously, the SINR can not be measured at any particular coherence block. As a result, the achievable SE in (18) and (19) are effectively equivalent to that of a

fading channel, where the CSI is perfectly known at the receiver.

In the centralized operation of the Cell-Free system, the received uplink signals are forwarded to the CPU through a fronthaul link. The CPU estimates the channels and selects the combining vector to detect the transmitted data. In the detection process, the optimal combining vector is the vector that maximizes the instantaneous SINR in (18) and (19). Since these expressions are generalized Rayleigh quotients with respect to $\boldsymbol{a}_k$, we consider three scalable linear detectors to maximize the SINR for UT k: Minimum Mean-Squared Error (MMSE), Regularized Zero-Forcing (RZF), and Maximum Ratio (MR). Table 2 summarizes the three combining detectors considered in this section, distinguishing between the case of Cell-Free and Co-Cellular system deployments.

Note that in Cell-Free system, the considered Partial-MMSE (PMMSE) detector is a scalable detector obtained from the optimal MMSE. The difference is that, in the approximated scalable PMMSE detector, the CPU uses only the signals transmitted from users sharing the same set of APs as UT k in the processing. Partial Regularized Zero-Forcing (PRZF) detector is an alternative detector with less complexity than scalable PMMSE. It can be obtained by neglecting the correlation matrix of the signals received by unknown channels in the PMMSE detector, i.e. $\sum_{i\in\mathcal{S}_k} p_i \mathbf{D}_k \mathbf{C}_{err} \mathbf{D}_k = 0$.

In the Large Scale Co-Cellular deployment, the combining process and data detection are carried out at the same place. The multi-cell MMSE (MC-MMSE) is an optimal detector for Co-Cellular deployment in the sense that it maximizes the expression (19). A simpler linear detector known as single-cell MMSE (SC-MMSE) can be obtained by considering an isolated BS that estimate channels and process signals only from its own UTs. It can be obtained by replacing the channel estimation statistics in the multi-cell MMSE detector with its average. Another detector with less complexity than SC-MMSE is a single-cell RZF (SC-RZF), which can be obtained by neglecting all the correlation matrices in the expression of SC-MMSE detector.

Due to the expectations in (18) and (19), the closed-form solution of the spectral efficiency (SE) can not be computed using the MMSE linear detector. Hence, we proceed numerically, using the Monte Carlo simulation approach to compute the SE for both system deployments.

IV. FRONTHAUL REQUIREMENTS

In practice, the achievable SE is limited by the capacity of the wireless channels and the capacity of the fronthaul links. Note that the Cell Free deployment with a centralized approach can reduce the fronthaul load compared to the cellular distributed LS-MU-MIMO systems. Further reduction can be achieved by enabling the local distributed implementation in the Cell-Free systems, where some processing is carried out at the APs. Motivated by this argument, this section investigates different local combining techniques for Cell-Free deployment with limited fronthaul capacity, taking into account the effects of imperfect CSI and spatially correlated fading.

Unlike the centralized implementation considered in section III, in the distributed operations, each AP exploits its received pilots and estimates the channels locally. The data detection in the distributed operation involves two layers. In the first layer, for each UT, the AP uses channel estimates to select a receive combining vector and then compute the local estimate of the transmitted data (Only this local data estimate will be sent to the CPU). In the second layer, the CPU decodes the transmitted data with the help of a large-scale fading decoding (LSFD) scheme, which involves the use of receiver weighting coefficient vectors. The CPU can find the optimized weights to maximize the SE. This process can be summarized as follows. Based on the received signal given in (2), an estimate of the transmitted data symbols can be obtained by applying a local linear combiner as

$$\hat{x}_{l,k} = \boldsymbol{a}_{l,k}\boldsymbol{y}_l^{CF} = \boldsymbol{a}_{l,k}^H \boldsymbol{h}_{l,k} x_k + \sum_{\substack{i=1 \\ i\neq k}}^{K} \boldsymbol{a}_{l,k}^H \boldsymbol{h}_{l,i} x_i + \boldsymbol{a}_{l,k}^H \boldsymbol{w}_l. \tag{21}$$

Based on the local estimation in (21), the CPU uses the LSFD weight vector $\left\{\mathbf{v}_{l,k} : l = 1, \ldots, L\right\}$ to centrally estimate the

$$SE_k^{CF} = \left(1 - \frac{\tau_p}{\tau_c}\right) \mathbb{E}\left\{log_2\left(1 + SINR_k^{CF}\right)\right\} \tag{18}$$

$$SE_k^{Co-Cell} = \left(1 - \frac{\tau_p}{\tau_c}\right) \mathbb{E}\left\{log_2\left(1 + SINR_k^{Co-Cell}\right)\right\} \tag{19}$$

$$SINR_k^{CF} = \frac{p_k \left|\boldsymbol{a}_k^H \boldsymbol{D}_k \hat{\boldsymbol{h}}_k\right|^2}{\sum_{\substack{i=1 \\ i\neq k}}^{K} p_i \left|\boldsymbol{a}_k^H \boldsymbol{D}_k \hat{\boldsymbol{h}}_i\right| + \boldsymbol{a}_k^H \left(\sum_{i=1}^{K} p_i \boldsymbol{D}_k \boldsymbol{C}_{err} \boldsymbol{D}_k\right) \boldsymbol{a}_k + \sigma^2 \left\|\boldsymbol{D}_k \boldsymbol{a}_k\right\|^2} \tag{20a}$$

$$SINR_k^{Co-Cell} = \frac{p_{jk} \left|\boldsymbol{a}_{jk}^H \hat{\boldsymbol{h}}_{j,jk}\right|^2}{\sum_{n=1}^{N} \sum_{\substack{i=1 \\ (n,i)\neq(j,k)}}^{K_n} p_{ni} \left|\boldsymbol{a}_{jk}^H \hat{\boldsymbol{h}}_{ni}^j\right| + \boldsymbol{a}_{jk}^H \left(\sum_{n=1}^{N} \sum_{i=1}^{K_n} p_{ni} \boldsymbol{C}_{err}\right) \boldsymbol{a}_{jk} + \boldsymbol{a}_{jk}^H \left(\sigma^2 \boldsymbol{I}_{M_j}\right) \boldsymbol{a}_{jk}} \tag{20b}$$

transmitted data as

$$\begin{aligned}\hat{x}_k &= \sum_{l=1}^{L} \boldsymbol{v}_{l,k}^{*} \hat{x}_{l,k}. \\ &= \sum_{l=1}^{L} \boldsymbol{v}_{l,k}^{*} \boldsymbol{a}_{l,k}^{H} \boldsymbol{h}_{l,k} x_k + \sum_{l=1}^{L} \boldsymbol{v}_{l,k}^{*} \boldsymbol{a}_{l,k}^{H} \sum_{\substack{i=1 \\ i \neq k}}^{K} \boldsymbol{h}_{l,i} x_i \\ &\quad + \sum_{l=1}^{L} \boldsymbol{v}_{l,k}^{*} \boldsymbol{a}_{l,k}^{H} \boldsymbol{w}_l \end{aligned} \tag{22}$$

Unlike the analysis in section III, we adopt a different capacity bound, where the achievable spectral efficiency of UT k is introduced in lemma 2.

Lemma 2: When using LMMSE channel estimation and linear processing, an achievable uplink SE of the k^{th} UT in a Cell-Free system with distributed implementation is given as (23), shown at the bottom of the page, with the effective SINR given in (24), *as shown at the bottom of the page.*

Proof: The proof follows from the same technique of lower-bounding adopted in [16]. The main differences between this capacity bound and the one in (18) are: 1) It can be applied for any channel fading distribution; and 2) The transmitted data can be detected as if transmitted over a non-fading channel with gain $\mathbb{E}\left\{\boldsymbol{a}_{l,k}^{H} \boldsymbol{D}_{l,k} \boldsymbol{h}_{l,k}\right\}$; hence, all the terms in (24) are deterministic and can be computed.

The expression in (24) can be further maximized by replacing the vector $\boldsymbol{a}_{l,k}^{H}$ in (22) with $\boldsymbol{a}_{l,k}^{H} \boldsymbol{D}_{l,k}$ and choose $\boldsymbol{v}_k$ as $\boldsymbol{v}_k = p_k \left(\sum_{i=1}^{K} p_i \left\{\boldsymbol{g}_{i,k} \boldsymbol{g}_{i,k}^{H}\right\} + \sigma^2 \boldsymbol{F}_k\right)$, which leads to the maximized effective SINR given as (25), *shown at the bottom of the page*, where, $\boldsymbol{D}_k = dig\left(\boldsymbol{D}_{1,k}, \ldots, \boldsymbol{D}_{1,k}\right)$, $\boldsymbol{g}_{i,k} = [\boldsymbol{a}_{1,k}^{H} \boldsymbol{D}_{1,k} \boldsymbol{h}_{1,k}, \ldots.., \boldsymbol{a}_{L,k}^{H} \boldsymbol{D}_{L,k} \boldsymbol{h}_{L,k}]^{\mathrm{T}}$, and $\boldsymbol{F}_{\mathrm{k}} = dig\left(\left\{\left\|\boldsymbol{D}_{1,k} \boldsymbol{a}_{1,k}^{H}\right\|\right\}, \ldots.., \left\{\left\|\boldsymbol{D}_{L,k} \boldsymbol{a}_{L,k}^{H}\right\|\right\}\right)$.

Similar to the analysis for the fully centralized operation, different combining schemes result in different spectral efficiencies and computational complexities. We consider two combining schemes with low signal processing complexity:

i) *Local Maximum Ratio (MR) Combining*, which has the lowest detection complexity. The MR combining vector constructed by the lAP for UTs in $\mathcal{Q}_k$ is given as

$$\boldsymbol{a}_{l,k}^{MR} = \boldsymbol{D}_{l,k} \hat{\boldsymbol{h}}_{l,k}. \tag{26}$$

It maximizes the receive signal power without taking into account the existence of other UTs. To make the system more performance-efficient, sophisticated combining schemes are employed to suppress the inter-user interference;

ii) *Local partial regularized ZF (LPRZF),* which gives better performance when there is interference from other UTs in the LS-MU-MIMO systems. This combining scheme provides weighting between interference suppression and maximizing the desired signal. Following the same arguments in [40], the LPRZF combining vector for user UT k at AP l is given as

$$\boldsymbol{a}_{l,k}^{LPRZF} = p_k \left(\sum_{i \in D_l} p_i \hat{\boldsymbol{h}}_{il} \hat{\boldsymbol{h}}_{il}^{H} + \sigma^2 I_{N_{AP}}\right)^{-1} \boldsymbol{D}_{kl} \hat{\boldsymbol{h}}_{kl}. \tag{27}$$

The matrix form of LPRZF, which gathers the combining vectors for all UTs can be written as

$$\boldsymbol{A}_{l,k}^{LPRZF} = \boldsymbol{D}_{kl} \hat{\boldsymbol{H}}_{D_l} \left(\hat{\boldsymbol{H}}_{D_l} \hat{\boldsymbol{H}}_{D_l}^{H} + \sigma^2 \boldsymbol{P}_{D_l}^{-1}\right)^{-1}. \tag{28}$$

where the matrix $\hat{\boldsymbol{H}}_{D_l}$ is constructed by stacking together all the vectors of the estimated channels $\hat{\boldsymbol{h}}_{il}$ having the indices $i \in D_l$, and $\mathbf{P}$ is a diagonal matrix containing all the transmit powers p_i for $i \in D_l$.

After combining with the LPRZF vectors, all the estimated signals will be sent to the CPU via fronthaul links. Then, the CPU applies the LSFD scheme to decode the transmitted data. By substituting (28) into (25), the achievable spectral efficiency of UT k is obtained by (23).

V. SPATIAL CORRELATION MODEL

This section aims to generate $\mathbf{R}_{\mathcal{X}}$ since the channel response $\mathbf{h}_{\mathcal{X}}$ is considered to have a correlated Rayleigh fading distribution modeled as $\mathbf{h}_{\mathcal{X}} \sim N_C\left(0, \mathbf{R}_{\mathcal{X}}\right)$, where $\mathbf{R}_{\mathcal{X}}$ is the correlation matrix of the channel response $\mathbf{h}_{\mathcal{X}}$. We consider a geometric-based channel model, which takes into account the correlation between antennas, the array geometry, and the distribution of the scatterers around users and APs (or BSs). Gaussian Local Scattering scheme, where the scattering process only happens around the UTs, is considered in this paper. Due to this scattering, the APs (or BSs) will receive the transmitted signal from different paths ($\mathcal{Z}$). The correlation matrix can be viewed as an expectation of all channel responses in all paths and written as [72]

$$\mathbf{R}_{\mathcal{X}} = \mathbb{E}\left\{\sum_{i=1}^{\mathcal{Z}} \boldsymbol{\alpha}_i \boldsymbol{\alpha}_i^{H}\right\}. \tag{29}$$

where $\boldsymbol{\alpha}_i$ represents the response of i^{th} path and for a particular (l, m) element of the $\mathbf{R}_{\mathcal{X}}$ matrix can be written as,

$$\begin{aligned}[\mathbf{R}]_{l,m} &= \sum_{i=1}^{N} \\ &\quad \times \mathbb{E}\left\{|g_i|^2\right\} \mathbb{E}\left\{e^{2j d_H (l-1) sin(\bar{\varphi}_i)} e^{-2j d_H (m-1) sin(\bar{\varphi}_i)}\right\} \end{aligned} \tag{30}$$

$$SE_k^{CF} = \left(1 - \frac{\tau_p}{\tau_c}\right) \mathbb{E}\left\{log_2\left(1 + SINR_k^{CF}\right)\right\} \tag{23}$$

$$SINR_k = \frac{p_k \left|\boldsymbol{v}_k^{H} \mathbb{E}\left\{\boldsymbol{g}_{k,k}\right\}\right|^2}{\sum_{i=1}^{K} p_i \mathbb{E}\left\{\left|\boldsymbol{v}_k^{H} \boldsymbol{g}_{i,k}\right|^2\right\} - p_k \left|\boldsymbol{v}_k^{H} \mathbb{E}\left\{\boldsymbol{g}_{k,k}\right\}\right|^2 + \boldsymbol{\sigma}^2 \boldsymbol{v}_k^{H} \boldsymbol{F}_k \boldsymbol{a}_k} \tag{24}$$

$$SINR_k = p_k \left\{\boldsymbol{g}_{k,k}^{H}\right\} \times \left(\sum_{i=1}^{K} p_i \left\{\boldsymbol{g}_{i,k} \boldsymbol{g}_{i,k}^{H}\right\} + \sigma^2 \boldsymbol{F}_k - p_k \mathbb{E}\left\{\boldsymbol{g}_{k,k}\right\} \mathbb{E}\left\{\boldsymbol{g}_{k,k}^{H}\right\}\right)^{-1} \left\{\boldsymbol{g}_{k,k}\right\} \tag{25}$$

where g_i denotes the average gain for the i^{th} multipath component that arrives from a certain angle $\overline{\varphi}$, and d_H represents the spacing between antenna elements.

Following the same definitions in [42], if the scatterers around the UTs are located in a Gaussian distribution, the spatial correlation matrix can be expressed as

$$[\mathbf{R}]_{l,m} = \sum_{i=1}^{N} \mathbb{E}\left\{|g_i|^2\right\} \int_{-\infty}^{\infty} e^{2jd_H(l-m)sin(\overline{\varphi})} \times \frac{1}{\sqrt{2\pi}\sigma_{\overline{\varphi}}} e^{-\frac{(\overline{\varphi}-\varphi)^2}{2\sigma_{\overline{\varphi}}^2}} d\overline{\varphi} \tag{31}$$

where $\sum_{i=1}^{\mathcal{Z}} \mathbb{E}\left\{|g_i|^2\right\}$ is the average gain of all multipath components. Further, by letting $\overline{\varphi} = \varphi + \vartheta$, (31) can be written in a more simplified form as,

$$[\mathbf{R}]_{l,m} = \beta \int_{-\infty}^{\infty} \mathrm{e}^{2jd_H(l-\mathrm{m})sin(\varphi+\vartheta)} \frac{1}{\sqrt{2\pi}\sigma_{\varphi}} \mathrm{e}^{-\frac{\vartheta^2}{2\sigma_{\varphi}^2}} d\vartheta \tag{32}$$

where $\beta = \sum_{i=1}^{N} \mathbb{E}\left\{|g_i|^2\right\}$, φ, ϑ and σ_{φ} are the nominal angle-of-arrive, the variation around the nominal angle and the angular standard deviation around the nominal angle, respectively.

VI. RESULTS AND DISCUSSION

In this section, the performance of Cell-Free and Co-Cellular LS-MU-MIMO systems is evaluated using Monte-Carlo simulations in different scenarios with different combining schemes. We focus on the transmission in the uplink scenario, and the transmit power of each UT is $p_k = 20\ dBm$. Further, the assumption of imperfect CSI (described in section III) is adopted for combining design. In the two network configurations, to maintain fairness in the comparison, settings, such as coverage area, total radiated power, user density, antenna density, and propagation model are set to be the same. We consider the system topologies shown in Fig. 2, where each network deployment is assumed to be deployed in a square area of 1000 m $\times$1000 m. This area is representative of a dense urban environment, which supports low-to-moderate mobility and channel dispersion. The coverage area is also assumed to be wrapped around at the edges to simulate an area with no boundaries and prevent any location-related issues.

In Cell-Free network deployment, the APs and the UTs are distributed in the area uniformly at random with density λ[L/km^2]. Unless stated otherwise, all APs and all UTs are equipped with a single antenna. Moreover, for Co-Cellular deployment, all BS antennas are co-located at the center of each cell. The BSs and the UTs are also uniformly placed randomly in the area, and each BS covers $\frac{1}{N} \times \frac{1}{N}$ square meters, with total network density $\lambda[\mathrm{M}_t/km^2]$, where M_t denotes the total number of antenna elements in the network.

In the simulation setups, the communication bandwidth B (in MHz), the carrier frequency f_0 (in GHz), and several other key system parameters that we have chosen are summarized in Table 3. The results in each figure have been averaged over 50 random setup realizations, and the locations of all APs, BSs, and UTs are generated independently in each system setup. This random realization of all APs, BSs, and UTs locations in both network configurations determines the large-scale fading coefficients in the network. The spatial correlation model given in section V is considered in all the simulations. The path loss model is used as given in [16], which is mathematically written as,

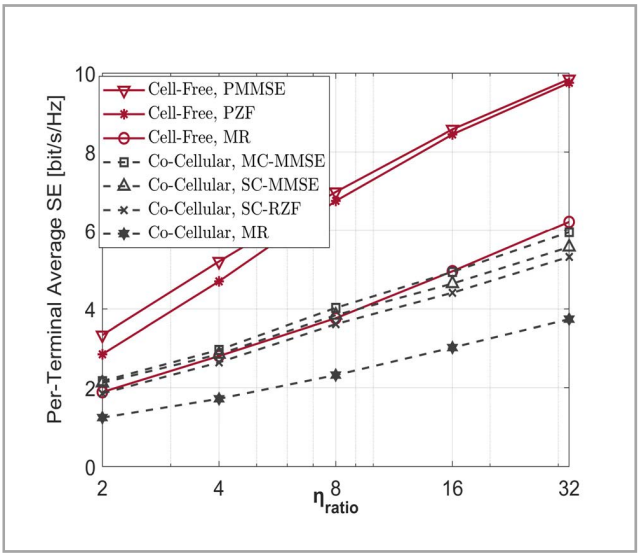

FIGURE 3. Per-Terminal Average SE as a function of η_{ratio} with total active UTs in the area K = 128. We consider the pilot length $\tau_p = 8$ and the angular standard deviation $\sigma_{\varphi} = 15$.

$$\beta_{\chi}\,[dB] = A_{d_0} - 10\gamma log_{10}\left(\frac{d_{\chi}}{d_0}\right) + F_{\chi}. \tag{33}$$

where A_{d_0} denotes the average channel gain at d_0 reference distance, γ is the path loss exponent, which determines how the distance will affect the path loss increasing; d_{χ} represents the separation distance, $F_{\chi} \sim \mathcal{N}\left(0, \sigma_{shadow}^2\right)$ is a zero-mean Gaussian distributed random variable, and the shadowing effect modeled by σ_{shadow}^2. In the following subsections, we define the system settings and present the corresponding simulation results. In Fig. 3 to Fig. 8, we focus on the system performance with a centralized implementation comparing the SE of Cell-Free and Co-Cellular using different system configurations: Antenna-UT ratios, pilot scaling factors, and network densities. Next, we consider the channel estimation quality of both network deployments and study the effect of increasing the Antenna-UT ratio on the channel estimation accuracy. Then, we investigate the impact of the channel spatial correlation on the system performance of Cell-Free and Co-Cellular network configurations and the uncorrelated channel model, where $\mathbf{R}_{\chi} = \beta_{\chi} I$ is considered as a reference for performance comparison. Finally, from Fig. 9 up to Fig. 11 we study the effect of distributed implementation on the system performance of Cell-Free system deployment and compare the result with the centralized implementation.

TABLE 3. System parameters for the simulation.

Parameter	Description
Total area of the network	1000m × 1000m
Bandwidth (B)	20 MHz
Carrier frequency	2 GHz
Path-loss exponent (γ)	3.8
Standard deviation of shadow fading	7.6 dB
Noise figure	7 dB
Receive noise power	-94 dB
Median channel gain at $1m$ (A_{d_0})	-30.5 dB
Reference distance (d_0)	1 m
Correlation distance	9 m
Antenna height at the UT	1.5 m
Antenna gains	0 dBi
UT transmit power p_k	100 mW
length of coherence block (τ_c) samples	400
Antenna height at the AP	10 m
Antenna height at the BS	25 m

A. PER-TERMINAL SE

Taking the achieved spectral efficiency as a system performance metric, this section aims to investigate and evaluate the performance of the system with different Antenna-UT ratios (η_{ratio}), pilot scaling factors (ζ), and network densities (λ). Hence, we compare the performance of Cell-Free and Co-Cellular system deployments as η_{ratio}, ζ, K, and λ increase with a constant ratio when a fully centralized implementation is used. Different linear detectors are considered during the simulations: PMMSE, PRZF, and MR for Cell-Free deployment; MC-MMSE, SC-MMSE, SC-RZF, and MR for Co-Cellular system deployment.

Note that with MR combining, the intra-cell interference is a drastic limiting factor for the achievable Per-Terminal SE regardless of the system deployment adopted. Therefore, due to their ability to suppress the inter-user interference, the MMSE and ZF significantly outperform the MR scheme in all approaches. The results show that the Cell-Free approach significantly outperforms the Co-located Cellular deployment in terms of uplink Per-Terminal SE with less performance variations. In the following subsections, we focus on the average Per-Terminal SE performance and compare the two system deployments as the Antenna-UT, pilot scaling factor, and network density grow larger.

1) ANTENNA-UT ANALYSIS

In LS-MU-MIMO systems, the number of antenna elements has to be large enough compared to the number of active users. The Antenna-UT ratio (η_{ratio}) is a key parameter in LS-MU-MIMO systems, which is defined as the ratio of the antenna elements to the active users. As mentioned in definitions 1 and 2, this ratio has to be larger than 1 in LS-MU-MIMO systems. We assume that the antenna-UT ratio taking the values as $\eta_{ratio} = 2^n$, where n $= [1, 2, \ldots, 5]$ for both system deployments. The total active terminals in the area are fixed ($K = 128$), $L = K \times \eta_{ratio}$, and $M_t = K \times \eta_{ratio}$ in the Cell-Free and Co-Cellular systems, respectively.

Based on η_{ratio}, Fig. 3 presents the achievable per-terminal spectral efficiency in the deployments of Cell-Free and Co-Cellular LS-MU-MIMO systems with the total number of active users $K = 128$. It can be seen that both systems offer better performance when the ratio of Antenna-UT (η_{ratio}) is increasing. The average Per-Terminal SE increases linearly with η_{ratio} in Cell-Free and Co-Cellular systems. In Cell-Free, the PMMSE and PRZF detectors provide almost the same Per-Terminal SE, especially when η_{ratio} grows higher. However, both detectors provide significantly higher SE compared to the MR detector.

For the Co-Cellular system, the MC-MMSE detector provides slightly better performance than SC-MMSE, and the SC-MMSE provides a slightly higher SE than SC-RZF when η_{ratio} is small. However, for large η_{ratio}, the largest SE is achieved by MC-MMSE. Also, in contrast to the Cell-free system, the gap in the performance between MMSE and RZF schemes increases as η_{ratio} grows higher.

2) PILOT SCALING ANALYSIS

In the LS-MU-MIMO systems, UTs that share the same pilots are the reason behind the pilot contamination effect. This effect is one of the challenges that limit the multi-cell LS-MU-MIMO system's performance. In Cell-free LS-MU-MIMO, an AP is allowed to serve up to UTS $= \tau_p$. Hence, large τ_p will result in a reduction in the pilot contamination. In the Co-Cellular, the pilot reuse mitigation process is considered, where the frequency of pilot reuse in the network is increased. Let ζ be the scaling factor ruling the length of the pilot in a Cell-Free system and determining the frequency of pilot reuse in the Co-Cellular system. This section illustrates the effect of scaling the pilot length on the system performance. In both network configurations, we can write the length of the pilot as

$$\tau_p = \zeta \times \tau_0. \tag{34}$$

where $\tau_0 = \frac{L}{K}$ and $\tau_0 = \frac{M_t}{K}$ in Cell-Free and Co-Cellular systems, respectively. Fig. 4 illustrates the Per-Terminal SE as a function of ζ for both network configurations. We choose $\zeta = 2^n$ where n $= [0, 1, \ldots, 4]$. As can be observed, different scaling factors achieve a different amount of Per-Terminal SE. In Cell-Free deployments, increasing ζ results in improvement in the Per-Terminal SE. This improvement can be interpreted as follows. Since the AP is only allowed to serve up to τ_p terminals, the increase in ζ will increase τ_p, allowing the AP to serve more UTs, which means less sharing to the same pilots and hence less pilot contamination. However, as can also be observed from Fig. 4, the increase in ζ after a certain limit no longer improves the Per-Terminal

TABLE 4. SE and ASE for cell-free and co-cellular systems with network density λ. We consider $\eta_{ratio} = 8$ for both systems.

Cell-Free							Co-Cellular						
$\lambda[L/km^2]$							$\lambda[M_t/km^2]$						
	L=256		L=1024		L=2048			M_t=256		M_t=1024		M_t=2048	
Scheme	SE	ASE	SE	ASE	SE	ASE	Scheme	SE	ASE	SE	ASE	SE	ASE
P-MMSE	6.2	198	7.1	909	6.7	1715	MC-MMSE	3.4	109	4.1	525	3.8	972
P-RZF	6.2	198	6.8	870	6.4	1638	SC-MMSE	3.4	109	3.9	499	3.6	921
MR	4.7	150	3.8	486	3.1	794	SC-RZF	3.4	109	3.7	473	3.4	870

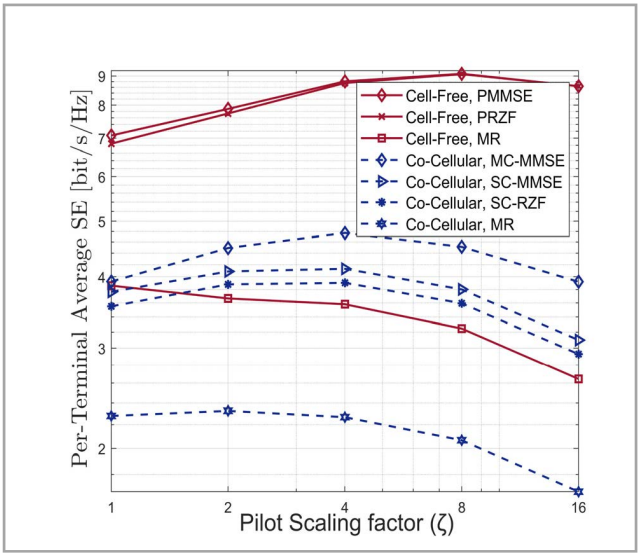

FIGURE 4. Per-Terminal Average SE as a function of pilot scaling factor ζ. The total UTs in the network $K = 128$ and the total of APs in Cell-Free and the antenna elements in Co-Cellular $L = M_t = 1024$. We consider $\tau_0 = 8$ and the angular standard deviation $\sigma_\varphi = 10$.

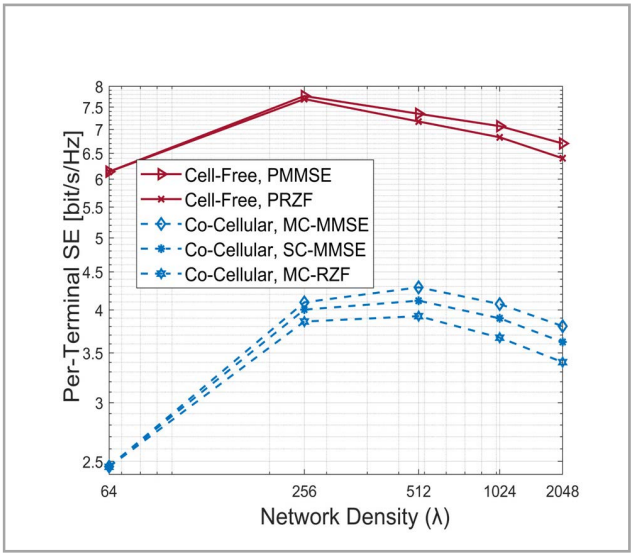

FIGURE 5. Per-Terminal Average SE vs. Network Density for 'Cell-Free and Cellular' LS-MU-MIMO deployments with $\eta_{ratio} = 8$.

SE, and performance degradation can be observed. The reason behind this is that higher values of ζ make the pilots consume a substantial portion of the available samples. Both linear detectors (PMMSE and PRZF) achieve almost the same SE in the Cell-Free system and substantially outperform MR. While Pmmse and PRZF achieve their best performance at $\zeta = 8$, mr achieves its best performance at $\zeta = 1$.

In Co-Cellular deployment, and similar to Cell-Free, improvement in SE can be observed when increasing ζ within a specific range. However, we can observe that there is a significant difference in the SE between all the detectors. Among all the considered detectors, MC-MMSE can achieve the largest SE, and its optimal pilot scaling factor (reuse factor) is $\zeta = 4$.

3) NETWORK DENSITY

This section aims to investigate the impact of network density on the system performance. For both system architectures, the network density (λ) can be realized by having many APs in the Cell-Free deployment (λ[L/km^2]) and many antenna elements in the Co-Cellular deployment (λ[M_t/km^2]). To maintain fairness in the comparison, the ratio of Antenna-UT (η_{ratio}) in Fig. 5 and 6 is fixed for each value of λ, i.e., as the number of APs (or antenna elements) increases, the number of UTs increases accordingly. Also, the density of APs (in Cell-Free), the density of antenna element (in Co-Cellular), and the UTs increase with a constant ratio. For example, for a fixed value of η_{ratio}, the density of the network increases in the form of $\lambda = 2^n$ and the total UTs in the form of $K = \frac{\lambda}{\eta_{ratio}}$. The simulation result in Fig. 5 is generated based on (18) and (19) for MMSE and RZF combining schemes in both network deployments. The achievable Per-Terminal average SE is plotted under different values of the network density and the number of active users K with a fixed ratio of Antenna-UT. As we can observe from this figure, the increase in the AP density (λ[L/km^2]) contributes more to the outperformance of Cell-Free deployment against Co-Cellular deployment with antenna element density (λ[M_t/km^2]). This outperform is a result of the cooperation among the APs, and the improvement of the coverage probability in the Cell-Free system as the AP density increases.

After a certain limit, the increase in the network density results in a non-increasing Pre-Terminal SE in both systems. The main reason for the SE decrease is the pilot contamination, which increases as the number of active users K increases and becomes more severe for higher values of λ.

In the Cell-Free system, the PMMSE achieves slightly better performance than PRZF with higher values of λ. For the Co-Cellular system, the three considered detectors achieve almost the same SE in less densified networks (smallλ).

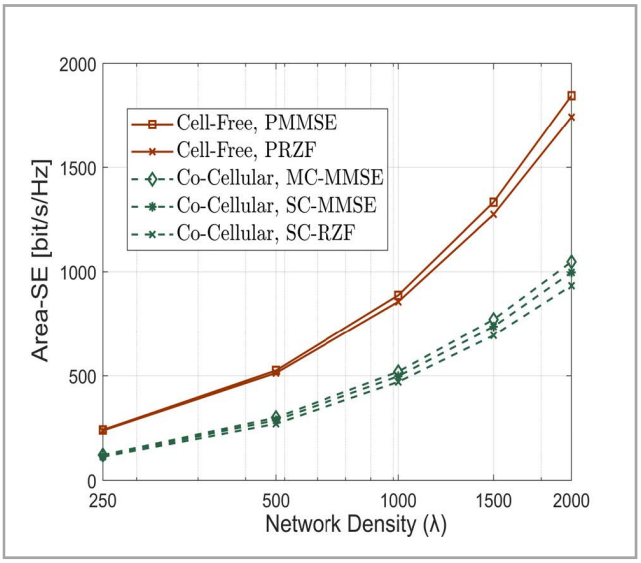

FIGURE 6. Area-SE vs. Network Density (λ) for 'Cell-Free and Cellular' LS-MU-MIMO deployments with $\eta_{\text{ratio}} = 8$.

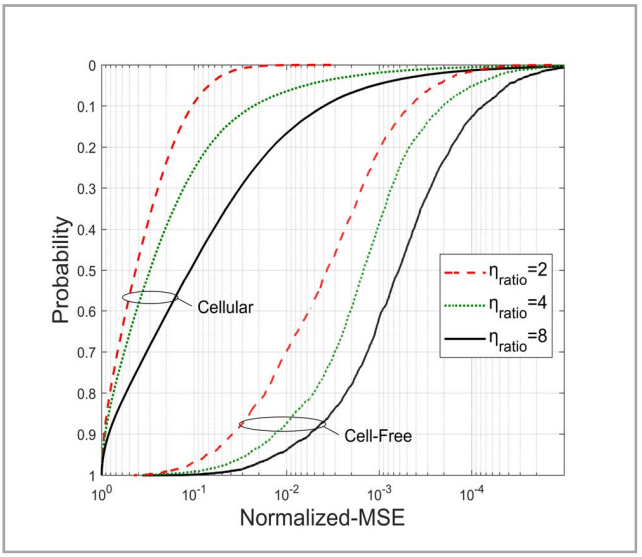

FIGURE 7. The empirical cumulative density function (CDF) of the normalized MSE in the channel estimation for an arbitrary UT. The result shown for different η_{ratio}, (Notice the reverse logarithmic scale). We consider $\tau_p = 10$ and the angular standard deviation $\sigma_\varphi = 10$.

However, the detectors are performed differently in higher network densities. Due to its ability to suppress the interference from different cells, the MC-MMSE has the best performance when λ grows higher.

Further, we consider the Area-Spectral Efficiency (ASE), which is defined as the sum of the SE of all UTs per unit area and mathematically can be written as,

$$\text{ASE} = \begin{cases} \dfrac{L}{\eta_{ratio}} \times \text{SE} & CF \\ \dfrac{M_t}{\eta_{ratio}} \times \text{SE} & Co-Cell \end{cases} \tag{35}$$

From Fig. 6, we can clearly see that both network deployments can achieve significant ASE as λ grows higher. However, one can observe that as the network density increases the performance gap between the two system deployments increases. This is basically due to two reasons: First, the network coverage provided by Cell-Free is always higher than Co-Cellular, which helps in eliminating the edge-users problem and results in a better ASE performance in Cell-Free system. Second, the Cell-Free system performs better than Co-Cellular when the multiuser interference increases.

Since the total number of active users K increases as λ increases in our ystem setup, the larger the number of active users, the higher the resultant interference. Cell-Free system deployment takes the advantage of the coordinated multi-point processing (CoMP), which is more robust at higher multiuser interference.

Table. 4 shows an example of the system performance variations on Per-Terminal SE and ASE with different network densities (λ). We also observe that while the Per-Terminal SE has a non-increasing behaviour with higher network densities, the ASE increases withλ.

B. CHANNEL ESTIMATION ACCURACY

Since the estimated channels include some estimation error (as stated in section III), in this section, we analyze the channel estimation accuracy of the investigated Cell-Free and Co-Cellular system configurations. We adopt a normalized mean square error ($\overline{MSE}$) as an accuracy metric for both systems, which is given as [27]

$$\overline{MSE}_\chi = \frac{\text{tr}\left(\mathbf{C}_\chi\right)}{\text{tr}\left(\mathbf{R}_\chi\right)}. \tag{36}$$

where the error correlation matrix $\mathbf{C}_\chi$ and the spatial correlation matrix $\mathbf{R}_\chi$ are defined as in section III.

Higher values of $\overline{MSE}$ mean that the channel estimation becomes less accurate. Fig. 7 shows the empirical probability CDF for a correlated channel as a function of the normalized MSE with different values of Antenna-UT (η_{ratio}).

When comparing the estimation accuracy of the two considered systems, we notice that a system with a large number of single-antenna distributed APs achieves better estimation accuracy than a system with a few numbers of BSs deployed with a large number of antenna elements. Hence, the Cell-Free deployment achieves better estimation accuracy than the Co-Cellular deployment. Moreover, it can be seen that the system with a higher η_{ratio} has smaller normalized MSE, which means that the estimation accuracy can be improved by adding more APs in the Cell-Free systems and more antenna elements in the Co-Cellular systems. This is a result of the key properties of LS-MU-MIMO system, i.e., channel hardening and favorable propagation.

C. CHANNEL CORRELATION EFFECT

Here we investigate the system's behaviour through Per-Terminal average SE achieved by an arbitrary UT according to the level of the channel correlation. Angular standard deviation (σ_φ) is the parameter for channel spatial correlation, and it reflects how correlated the channels are. Channels with higher correlation have small σ_φ, and vice versa.

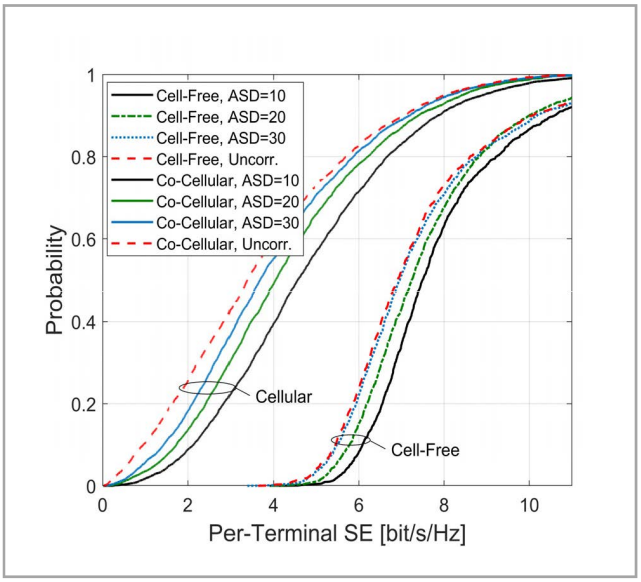

FIGURE 8. Cumulative Distribution Function (CDF) as a function of Per-Terminal average SE for minimum mean-squared error (MMSE) combiner, with $L = M_t = 256$, $K = 32$, and $\tau_p = 10$.

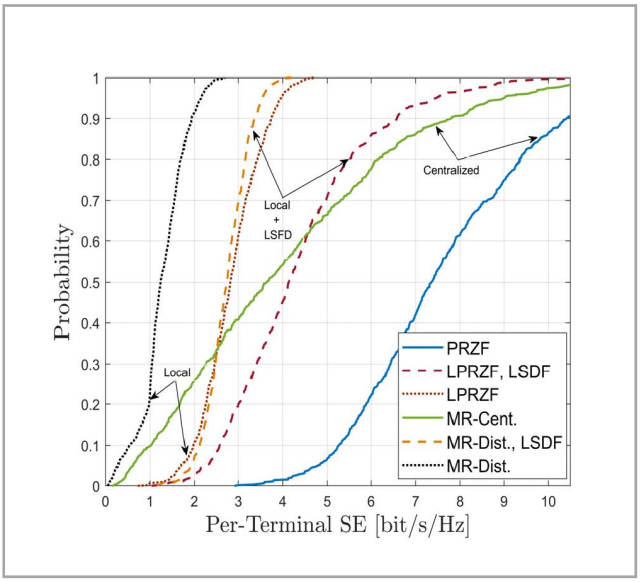

FIGURE 9. The empirical cumulative density function (CDF) for an arbitrary UT as a function of Per-Terminal average SE. We consider $L = 256$, $K = 32$, $\tau_p = 8$ and the angular standard deviation $\sigma_\varphi = 10$.

Fig. 8 shows the comparison between the two considered LS-MU-MIMO system architectures, taking into account the difference in the spatial distribution of APs (in Cell-Free), and antenna elements (in Co-Cellular). It shows the cumulative distribution as a function of Per-Terminal SE for PMMSE and MC-MMSE combining schemes in Cell-Free and Co-Cellular network deployments, respectively. Each AP in the Cell-Free system is equipped with 4 antennas, and the total antenna elements in both systems $L = M_t = 256$. We observe that a higher Per-Terminal SE can be achieved as the level of the channel correlation increases (small σ_φ). In contrast, as σ_φ increases, the channels become closer to the uncorrelated case, hence less Per-Terminal SE. The reason is that the channel estimation accuracy decreases as the spatial correlation decreases.

D. CELL-FREE DISTRIBUTED PROCESSING

At the cost of extra fronthaul traffic, the highest Per-Terminal SE is achieved in centralized processing, where the channel statistics are sent to the CPU. However, to alleviate the burden on the fronthaul links, the distributed implementation, where the processing is rather carried out locally at the APs, is investigated in this section. Unless stated otherwise, the simulation settings are the same as presented for the centralized implementation. In all the experiments, each UT is served by a limited set of APs located around it.

For Cell-Free deployment, Fig. 9-11 show a performance comparison for the following implementations: 1) Fully centralized, where APs forward data and CSI to the CPU; hence, the channel estimation and data detection are carried out at the CPU. 2) Local Distributed (one stage), where channels and data estimation are carried out locally at the APs; therefore, only local data estimates forwarded to the CPU and not the CSI. 3) Local Distributed (Two stages): where the CPU performs another round of data estimation, using the local data estimates forwarded by APs.

The results for different distributed detection schemes are obtained through Monte Carlo simulations, and the centralized case is shown as a reference case. For all Cell-Free implementations, two detection schemes are considered: LPZF and MR combining schemes. In the following, simulation results are shown in terms of Cumulative Distribution Function (CDF) for an arbitrary UT and in terms of average Per-Terminal SE as the number of APs and the scaling factor grow higher.

For a better understanding of the effect of the combining schemes on all implementations' comparison, Fig. 9 plotted the empirical cumulative distribution as a function of the Per-Terminal uplink SE. The simulation results are presented for fully centralized, local, and local with LSFD distributed implementations under the same fronthaul limits. The total active UTs in the area $K = 32$, $L = 256$, and $\tau_p = 8$. We also assume that each AP is equipped with a single antenna in all the implementations. It can be observed that the gap in the performance between the ZF-based and MR-based schemes is significant and different for each system implementation. The reason is the lack of ability to suppress the multiuser interference in the MR combining schemes. For example, compared with MR combining in the distributed implementation, LPRZF scheme gives around 40% higher improvement in the Per-Terminal SE. Furthermore, Fig. 9 shows that the performance of the LPRZF and MR can be significantly improved by adding LSFD as a second detection stage at the CPU.

Fig. 10 illustrates the effect of pilot length scaling on the achieved performance when the local distributed detection approaches are employed. We assume that each AP is equipped with a single antenna, the total active users $K = 128$, and the total number of APs in the network $L = 1024$.

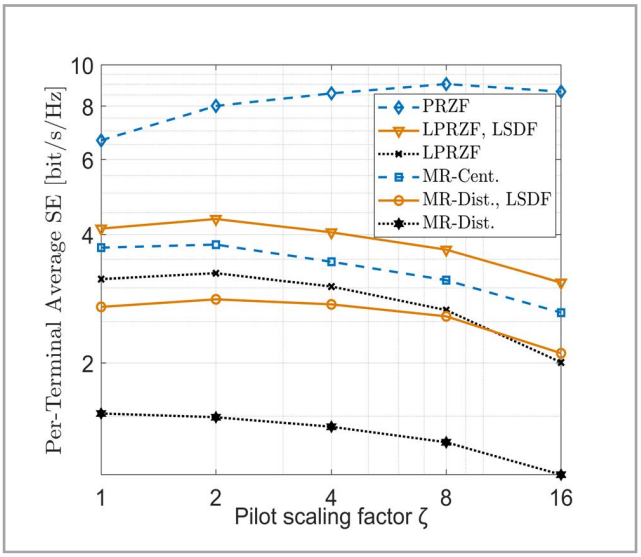

FIGURE 10. Per-Terminal Average SE as a function of pilot scaling factor ζ. The total UTs in the network $K = 128$ and the total APs $L = 1024$. We consider $\tau_0 = 8$ and the angular standard deviation $\sigma_\varphi = 10$.

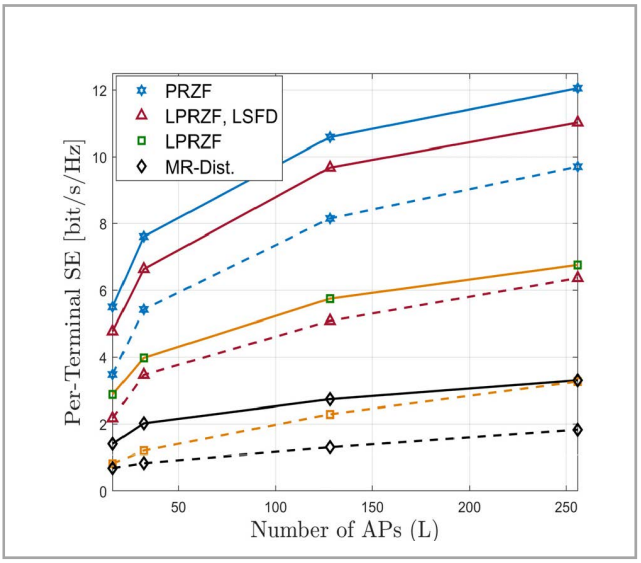

FIGURE 11. Per-Terminal Average SE as a function of the number of APs (L). The total UTs in the network $K = 8$. We consider $\tau_0 = 8$ and the angular standard deviation $\sigma_\varphi = 10$.

As mentioned earlier, scaling the pilot length will result in a reduction in the pilot reuse; therefore, the pilot contamination is reduced. Thus, the achieved SE performance's improvement continues up to a certain point. As can be seen in the figure, different combining schemes have different saturation points, after which the performance starts declining with more increase in the scaling factor. The saturation points of the centralized schemes (PRZF and MR-Cent.) are 8 and 2, respectively. For the distributed implementation, the two schemes (LRZF and MR-Dist.) are saturated at 2, when LSDF is used as a second stage detection. On the other hand, the two schemes are saturated at 2 and 1, when LSDF is not used.

Focusing on the average uplink SE, Fig. 11 depicts the Per-Terminal SE of PRZF, LPRZF, and MR as a function of the number of APs. We assume that the total active users $K = 8$, the number of APs (L) increases with a constant ratio, and each AP is equipped with either one antenna (dashed line) or four antennas (solid line). As can be observed from the figure, a substantial gain in the average Per-Terminal SE can be achieved for all schemes as the number of APs (L) grows. This is a result of the increase in the diversity gain when the number of APs increases. In addition, we can observe that PRZF, LPRZF and LPRZF with LSFD schemes gain more improvement in the performance compared to the MR scheme as the number of APs increases. This is expected due to the ability of ZF-based schemes to suppress the interference, which becomes more severe as the channel gain of other UTs increases. Compared to other combining schemes in the distributed implementation, LPRZF with LSFD provides the highest Per-Terminal SE.

The results in Fig. 11 show that deploying each AP with four antennas (solid line curves) instead of a single antenna (dashed line curves) increases the average Per-Terminal SE. This is because the increase in APs' antennas improves the ability to suppress the interference; as a result, per-terminal SE is increased.

VII. CONCLUSION

The paper has presented a comparative study of Cell-Free and Co-located Cellular LS-MU-MIMO deployments, given the same network density in a dense urban environment. In both system configurations, to achieve a good performance, many factors have to be taken into account, such as the Antenna-UT ratio, the correlation between the channel coefficients, channel estimation, antenna elements density, and pilot design. Considering more realistic scenarios, several simulations were carried out to evaluate and highlight the uplink performance of the two deployments. Compared to Co-Cellular LS-MU-MIMO systems, simulation results show that Cell-Free LS-MU-MIMO systems can significantly improve the achieved uplink performance, and this improvement becomes more noticeable as the number of APs grows higher. Moreover, for a given number of active UTs, a Cell-Free system can provide higher Per-Terminal SE while ensuring robust and uniform connectivity for all UTs (i.e., less performance variations). It is also clear that MMSE and RZF can achieve almost the same performance in a low-to-moderate densified network. However, among all the considered detectors, MMSE has the best performance when the network is more densified in Cell-Free and Co-Cellular systems. Moreover, the results also confirm that channel estimation accuracy in the correlated fading is higher than uncorrelated fading and can be improved further with a higher ratio of Antenna-UT. Finally, numerical results indicate that, in the distributed implementation of the Cell-Free system, the two-stage detection, (i.e., local schemes with LSDF), outperform the other schemes, and further improvement can be achieved by deploying the APs with more antennas.

REFERENCES

[1] C.-X. Wang, F. Haider, X. Gao, X.-H. You, Y. Yang, D. Yuan, H. M. Aggoune, H. Haas, S. Fletcher, and E. Hepsaydir, "Cellular architecture and key technologies for 5G wireless communication networks," *IEEE Commun. Mag.*, vol. 52, no. 2, pp. 122–130, Feb. 2014.

[2] A. Osseiran, F. Boccardi, V. Braun, K. Kusume, P. Marsch, M. Maternia, O. Queseth, M. Schellmann, H. Schotten, H. Taoka, H. Tullberg, M. A. Uusitalo, B. Timus, and M. Fallgren, "Scenarios for 5G mobile and wireless communications: The vision of the METIS project," *IEEE Commun. Mag.*, vol. 52, no. 5, pp. 26–35, May 2014.

[3] S. Buzzi, I. Chih-Lin, T. E. Klein, H. V. Poor, C. Yang, and A. Zappone, "A survey of energy-efficient techniques for 5G networks and challenges ahead," *IEEE J. Sel. Areas Commun.*, vol. 34, no. 4, pp. 697–709, Apr. 2016.

[4] J. G. Andrews, S. Buzzi, W. Choi, S. V. Hanly, A. Lozano, A. C. K. Soong, and J. C. Zhang, "What will 5G be?" *IEEE J. Sel. Areas Commun.*, vol. 32, no. 6, pp. 1065–1082, Jun. 2014.

[5] M. Shafi, A. F. Molisch, P. J. Smith, T. Haustein, P. Zhu, P. De Silva, F. Tufvesson, A. Benjebbour, and G. Wunder, "5G: A tutorial overview of standards, trials, challenges, deployment, and practice," *IEEE J. Sel. Areas Commun.*, vol. 35, no. 6, pp. 1201–1221, Jun. 2017.

[6] E. G. Larsson, O. Edfors, F. Tufvesson, and T. L. Marzetta, "Massive MIMO for next generation wireless systems," *IEEE Commun. Mag.*, vol. 52, no. 2, pp. 186–195, Feb. 2014.

[7] E. Björnson, L. Sanguinetti, H. Wymeersch, J. Hoydis, and T. L. Marzetta, "Massive MIMO is a reality—What is next? Five promising research directions for antenna arrays," *Digit. Signal Process.*, vol. 94, pp. 3–20, Nov. 2019.

[8] W. Liu, S. Han, C. Yang, and C. Sun, "Massive MIMO or small cell network: Who is more energy efficient?" in *Proc. IEEE Wireless Commun. Netw. Conf. Workshops (WCNCW)*, Apr. 2013, pp. 24–29.

[9] G. N. Kamga, M. Xia, and S. Aïssa, "Spectral-efficiency analysis of massive MIMO systems in centralized and distributed schemes," *IEEE Trans. Commun.*, vol. 64, no. 5, pp. 1930–1941, May 2016.

[10] E. Björnson, L. Sanguinetti, and M. Kountouris, "Deploying dense networks for maximal energy efficiency: Small cells meet massive MIMO," *IEEE J. Sel. Areas Commun.*, vol. 34, no. 4, pp. 832–847, Apr. 2016.

[11] W. Choi and J. G. Andrews, "Downlink performance and capacity of distributed antenna systems in a multicell environment," *IEEE Trans. Wireless Commun.*, vol. 6, no. 1, pp. 69–73, Jan. 2007.

[12] D. Wang, J. Wang, X. You, Y. Wang, M. Chen, and X. Hou, "Spectral efficiency of distributed MIMO systems," *IEEE J. Sel. Areas Commun.*, vol. 31, no. 10, pp. 2112–2127, Oct. 2013.

[13] R. Irmer, H. Droste, P. Marsch, M. Grieger, G. Fettweis, S. Brueck, H.-P. Mayer, L. Thiele, and V. Jungnickel, "Coordinated multipoint: Concepts, performance, and field trial results," *IEEE Commun. Mag.*, vol. 49, no. 2, pp. 102–111, Feb. 2011.

[14] J. Zhang, E. Bjornson, M. Matthaiou, D. W. K. Ng, H. Yang, and D. J. Love, "Prospective multiple antenna technologies for beyond 5G," *IEEE J. Sel. Areas Commun.*, vol. 38, no. 8, pp. 1637–1660, Aug. 2020.

[15] V. Jungnickel, K. Manolakis, W. Zirwas, B. Panzner, V. Braun, M. Lossow, M. Sternad, R. Apelfrojd, and T. Svensson, "The role of small cells, coordinated multipoint, and massive MIMO in 5G," *IEEE Commun. Mag.*, vol. 52, no. 5, pp. 44–51, May 2014.

[16] Ö. T. Demir, E. Björnson, and L. Sanguinetti, "Foundations of user-centric cell-free massive MIMO," *Found. Trends Signal Process.*, vol. 14, nos. 3–4, pp. 162–472, 2021.

[17] S. Elhoushy and W. Hamouda, "Performance of distributed massive MIMO and small-cell systems under hardware and channel impairments," *IEEE Trans. Veh. Technol.*, vol. 69, no. 8, pp. 8627–8642, Aug. 2020.

[18] G. Interdonato, E. Björnson, H. Q. Ngo, P. Frenger, and E. G. Larsson, "Ubiquitous cell-free massive MIMO communications," *EURASIP J. Wireless Commun. Netw.*, vol. 2019, p. 197, Dec. 2019.

[19] E. Björnson, E. G. Larsson, and T. L. Marzetta, "Massive MIMO: Ten myths and one critical question," *IEEE Commun. Mag.*, vol. 54, no. 2, pp. 114–123, Feb. 2016.

[20] T. L. Marzetta, "Noncooperative cellular wireless with unlimited numbers of base station antennas," *IEEE Trans. Wireless Commun.*, vol. 9, no. 11, pp. 3590–3600, Nov. 2010.

[21] H. Q. Ngo, E. G. Larsson, and T. L. Marzetta, "Energy and spectral efficiency of very large multiuser MIMO systems," *IEEE Trans. Commun.*, vol. 61, no. 4, pp. 1436–1449, Apr. 2013.

[22] J. Hoydis, S. T. Brink, and M. Debbah, "Massive MIMO in the UL/DL of cellular networks: How many antennas do we need?" *IEEE J. Sel. Areas Commun.*, vol. 31, no. 2, pp. 160–171, Feb. 2013.

[23] F. Rusek, D. Persson, B. K. Lau, E. G. Larsson, T. L. Marzetta, O. Edfors, and F. Tufvesson, "Scaling up MIMO: Opportunities and challenges with very large arrays," *IEEE Signal Process. Mag.*, vol. 30, no. 1, pp. 40–60, Jan. 2013.

[24] O. Ozdogan, E. Bjornson, and E. G. Larsson, "Massive MIMO with spatially correlated Rician fading channels," *IEEE Trans. Commun.*, vol. 67, no. 5, pp. 3234–3250, May 2019.

[25] L. Sanguinetti, E. Bjornson, and J. Hoydis, "Toward massive MIMO 2.0: Understanding spatial correlation, interference suppression, and pilot contamination," *IEEE Trans. Commun.*, vol. 68, no. 1, pp. 232–257, Jan. 2020.

[26] V. Raghavan and A. M. Sayeed, "Sublinear capacity scaling laws for sparse MIMO channels," *IEEE Trans. Inf. Theory*, vol. 57, no. 1, pp. 345–364, Jan. 2011.

[27] A. Alammari and M. Sharique, "Spatial channel correlation for local scattering with linear MMSE-based estimator and detector in multi-cell large scale MU-MIMO networks," *Trans. Emerg. Telecommun. Technol.*, vol. 32, no. 12, Dec. 2021, Art. no. e4366.

[28] F. Mirhosseini, A. Tadaion, and S. M. Razavizadeh, "Spectral efficiency of dense multicell massive MIMO networks in spatially correlated channels," *IEEE Trans. Veh. Technol.*, vol. 70, no. 2, pp. 1307–1316, Feb. 2021.

[29] A. Adhikary, A. Ashikhmin, and T. L. Marzetta, "Uplink interference reduction in large-scale antenna systems," *IEEE Trans. Commun.*, vol. 65, no. 5, pp. 2194–2206, May 2017.

[30] X. Li, E. Björnson, E. G. Larsson, S. Zhou, and J. Wang, "Massive MIMO with multi-cell MMSE processing: Exploiting all pilots for interference suppression," *EURASIP J. Wireless Commun. Netw.*, vol. 2017, no. 1, pp. 117–148, Dec. 2017.

[31] K. Guo, Y. Guo, G. Fodor, and G. Ascheid, "Uplink power control with MMSE receiver in multi-cell MU-massive-MIMO systems," in *Proc. IEEE ICC*, Jun. 2014, pp. 5184–5190.

[32] N. Krishnan, R. D. Yates, and N. B. Mandayam, "Uplink linear receivers for multi-cell multiuser MIMO with pilot contamination: Large system analysis," *IEEE Trans. Wireless Commun.*, vol. 13, no. 8, pp. 4360–4373, Aug. 2014.

[33] L. Dai, "A comparative study on uplink sum capacity with co-located and distributed antennas," *IEEE J. Sel. Areas Commun.*, vol. 29, no. 6, pp. 1200–1213, Jun. 2011.

[34] Z. Liu and L. Dai, "A comparative study of downlink MIMO cellular networks with co-located and distributed base-station antennas," *IEEE Trans. Wireless Commun.*, vol. 13, no. 11, pp. 6259–6274, Nov. 2014.

[35] J. Wang and L. Dai, "Asymptotic rate analysis of downlink multi-user systems with co-located and distributed antennas," *IEEE Trans. Wireless Commun.*, vol. 14, no. 6, pp. 3046–3058, Jun. 2015.

[36] M. Bashar, K. Cumanan, A. G. Burr, H. Q. Ngo, and M. Debbah, "Cell-free massive MIMO with limited backhaul," in *Proc. IEEE Int. Conf. Commun. (ICC)*, May 2018, pp. 1–7.

[37] Ö. Özdogan, E. Björnson, and J. Zhang, "Performance of cell-free massive MIMO with Rician fading and phase shifts," *IEEE Trans. Wireless Commun.*, vol. 18, no. 11, pp. 5299–5315, Nov. 2019.

[38] H. Q. Ngo, A. Ashikhmin, H. Yang, E. G. Larsson, and T. L. Marzetta, "Cell-free massive MIMO versus small cells," *IEEE Trans. Wireless Commun.*, vol. 16, no. 3, pp. 1834–1850, Mar. 2017.

[39] A. Papazafeiropoulos, P. Kourtessis, M. D. Renzo, S. Chatzinotas, and J. M. Senior, "Performance analysis of cell-free massive MIMO systems: A stochastic geometry approach," *IEEE Trans. Veh. Technol.*, vol. 69, no. 4, pp. 3523–3537, Apr. 2020.

[40] J. Zhang, J. Zhang, E. Björnson, and B. Ai, "Local partial zero-forcing combining for cell-free massive MIMO systems," *IEEE Trans. Commun.*, vol. 69, no. 12, pp. 8459–8472, Dec. 2021.

[41] Z. Chen and E. Björnson, "Channel hardening and favorable propagation in cell-free massive MIMO with stochastic geometry," *IEEE Trans. Commun.*, vol. 66, no. 11, pp. 5205–5219, Nov. 2018.

[42] S.-N. Jin, D.-W. Yue, and H. H. Nguyen, "Spectral and energy efficiency in cell-free massive MIMO systems over correlated Rician fading," *IEEE Syst. J.*, vol. 15, no. 2, pp. 2822–2833, Jun. 2021.

[43] T. H. Nguyen, T. K. Nguyen, H. D. Han, and V. D. Nguyen, "Optimal power control and load balancing for uplink cell-free multi-user massive MIMO," *IEEE Access*, vol. 6, pp. 14462–14473, 2018.

[44] E. Nayebi, A. Ashikhmin, T. L. Marzetta, H. Yang, and B. D. Rao, "Precoding and power optimization in cell-free massive MIMO systems," *IEEE Trans. Wireless Commun.*, vol. 16, no. 7, pp. 4445–4459, Jul. 2017.

[45] P. Liu, K. Luo, D. Chen, and T. Jiang, "Spectral efficiency analysis of cell-free massive MIMO systems with zero-forcing detector," *IEEE Trans. Wireless Commun.*, vol. 19, no. 2, pp. 795–807, Feb. 2020.

[46] E. Nayebi, A. Ashikhmin, T. L. Marzetta, and H. Yang, "Cell-free massive MIMO systems," in *Proc. 49th Asilomar Conf. Signals, Syst. Comput.*, Nov. 2015, pp. 695–699.

[47] S. Buzzi and C. D'Andrea, "Cell-free massive MIMO: User-centric approach," *IEEE Wireless Commun. Lett.*, vol. 6, no. 6, pp. 706–709, Dec. 2017.

[48] S. Buzzi, C. D'Andrea, A. Zappone, and C. D'Elia, "User-centric 5G cellular networks: Resource allocation and comparison with the cell-free massive MIMO approach," *IEEE Trans. Wireless Commun.*, vol. 19, no. 2, pp. 1250–1264, Feb. 2020.

[49] S. Chen, J. Zhang, J. Zhang, E. Björnson, and B. Ai, "A survey on user-centric cell-free massive MIMO systems," Dec. 2021, *arXiv:2104.13667*.

[50] G. Interdonato, P. Frenger, and E. G. Larsson, "Scalability aspects of cell-free massive MIMO," in *Proc. IEEE Int. Conf. Commun. (ICC)*, May 2019, pp. 1–6.

[51] E. Björnson and L. Sanguinetti, "Scalable cell-free massive MIMO systems," *IEEE Trans. Commun.*, vol. 68, no. 7, pp. 4247–4261, Jul. 2020.

[52] H. A. Ammar, R. Adve, S. Shahbazpanahi, G. Boudreau, and K. V. Srinivas, "User-centric cell-free massive MIMO networks: A survey of opportunities, challenges and solutions," 2021, *arXiv:2104.14589*.

[53] J. Zhang, S. Chen, Y. Lin, J. Zheng, B. Ai, and L. Hanzo, "Cell-free massive MIMO: A new next-generation paradigm," *IEEE Access*, vol. 7, pp. 99878–99888, 2019.

[54] M. Bashar, K. Cumanan, A. G. Burr, M. Debbah, and H. Q. Ngo, "Enhanced max-min SINR for uplink cell-free massive MIMO systems," in *Proc. IEEE ICC*, May 2018, pp. 1–7.

[55] A. Burr, M. Bashar, and D. Maryopi, "Cooperative access networks: Optimum fronthaul quantization in distributed massive MIMO and cloud RAN," in *Proc. IEEE VTC*, Jun. 2018, pp. 1–7.

[56] L. D. Nguyen, T. Q. Duong, H. Q. Ngo, and K. Tourki, "Energy efficiency in cell-free massive MIMO with zero-forcing precoding design," *IEEE Commun. Lett.*, vol. 21, no. 8, pp. 1871–1874, Aug. 2017.

[57] M. Bashar, H. Q. Ngo, K. Cumanan, A. G. Burr, P. Xiao, E. Bjornson, and E. G. Larsson, "Uplink spectral and energy efficiency of cell-free massive MIMO with optimal uniform quantization," *IEEE Trans. Commun.*, vol. 69, no. 1, pp. 223–245, Jan. 2021.

[58] G. Femenias and F. Riera-Palou, "Cell-free millimeter-wave massive MIMO systems with limited fronthaul capacity," *IEEE Access*, vol. 7, pp. 44596–44612, 2019.

[59] E. Nayebi, A. Ashikhmin, T. L. Marzetta, and B. D. Rao, "Performance of cell-free massive MIMO systems with MMSE and LSFD receivers," in *Proc. 50th Asilomar Conf. Signals, Syst. Comput.*, Nov. 2016, pp. 203–207.

[60] W. Fan, J. Zhang, E. Bjornson, S. Chen, and Z. Zhong, "Performance analysis of cell-free massive MIMO over spatially correlated fading channels," in *Proc. IEEE Int. Conf. Commun.*, May 2019, pp. 1–6.

[61] G. Interdonato, M. Karlsson, E. Björnson, and E. G. Larsson, "Local partial zero-forcing precoding for cell-free massive MIMO," *IEEE Trans. Wireless Commun.*, vol. 19, no. 7, pp. 4758–4774, Jul. 2020.

[62] J. Zhang, J. Zhang, D. W. K. Ng, S. Jin, and B. Ai, "Improving sum-rate of cell-free massive MIMO with expanded compute-and-forward," *IEEE Trans. Signal Process.*, vol. 70, pp. 202–215, 2022.

[63] S. Buzzi, C. D'Andrea, and C. D'Elia, "User-centric cell-free massive MIMO with interference cancellation and local ZF downlink precoding," in *Proc. 15th Int. Symp. Wireless Commun. Syst. (ISWCS)*, Aug. 2018, pp. 1–5.

[64] E. Björnson and L. Sanguinetti, "Making cell-free massive MIMO competitive with MMSE processing and centralized implementation," *IEEE Trans. Wireless Commun.*, vol. 19, no. 1, pp. 77–90, Jan. 2020.

[65] E. Bjornson and L. Sanguinetti, "Cell-free versus cellular massive MIMO: What processing is needed for cell-free to win?" in *Proc. IEEE 20th Int. Workshop Signal Process. Adv. Wireless Commun. (SPAWC)*, Jul. 2019, pp. 1–5.

[66] O. T. Demir and E. Björnson, "Joint power control and LSFD for wireless-powered cell-free massive MIMO," *IEEE Trans. Wireless Commun.*, vol. 20, no. 3, pp. 1756–1769, Mar. 2021.

[67] Ö. Özdogan, E. Björnson, and J. Zhang, "Cell-free massive MIMO with Rician fading: Estimation schemes and spectral efficiency," in *Proc. 52nd Asilomar Conf. Signals, Syst., Comput.*, 2018, pp. 975–979.

[68] Y. Xin, D. Wang, J. Li, H. Zhu, J. Wang, and X. You, "Area spectral efficiency and area energy efficiency of massive MIMO cellular systems," *IEEE Trans. Veh. Technol.*, vol. 65, no. 5, pp. 3243–3254, May 2016.

[69] A. Alammouri, J. G. Andrews, and F. Baccelli, "A unified asymptotic analysis of area spectral efficiency in ultradense cellular networks," *IEEE Trans. Inf. Theory*, vol. 65, no. 2, pp. 1236–1248, Feb. 2019.

[70] S. M. Yu and S.-L. Kim, "Downlink capacity and base station density in cellular networks," *Proc. IEEE WiOpt*, May 2013, pp. 119–124.

[71] Z. H. Shaik, E. Björnson, and E. G. Larsson, "MMSE-optimal sequential processing for cell-free massive MIMO with radio stripes," *IEEE Trans. Commun.*, vol. 69, no. 11, pp. 7775–7789, Nov. 2021.

[72] E. Björnson, E. G. Larsson, and M. Debbah, "Massive MIMO for maximal spectral efficiency: How many users and pilots should be allocated?" *IEEE Trans. Wireless Commun.*, vol. 15, no. 2, pp. 1293–1308, Feb. 2016.

[73] E. Björnson, J. Hoydis, and L. Sanguinetti, "Massive MIMO networks: Spectral, energy, and hardware efficiency," *Found. Trends Signal Process.*, vol. 11, nos. 3–4, pp. 154–655, 2017.

[74] T. H. Nguyen, T. V. Chien, H. Q. Ngo, X. N. Tran, and E. Bjornson, "Pilot assignment for joint uplink-downlink spectral efficiency enhancement in massive MIMO systems with spatial correlation," *IEEE Trans. Veh. Technol.*, vol. 70, no. 8, pp. 8292–8297, Aug. 2021.

AMR A. ALAMMARI received the B.Tech. degree in electronic engineering (communication division) from IBB University, Ibb, Yemen, in 2009, and the M.Tech. degree (Hons.) in electronics and communication engineering from JNTUH, Hyderabad, India, in 2016. He is currently a Research Scholar with the Department of Electronics Engineering, AMU, Aligarh, India. He is also working on large scale MU-MIMO transceiver design for 5G and beyond wireless systems. His research interests include wireless communication technologies with a focus on 5G/6G wireless systems.

MOHD SHARIQUE received the Ph.D. degree from the Indian Institute of Technology, Kanpur, in 2015. His broad area of research is waveform shaping methods for wireless communication, communication theory, massive MIMO, 5G, and beyond communication systems. He is currently supervising two Ph.D. students in the area of wireless communication systems. He has supervised seven M.Tech. dissertations and also supervises two M.Tech. dissertations. He is working on the application of learning theory in the area of massive MIMO for low complexity detection. Another problem he is working on is to reduce the overhead and complexity of channel estimation as well as pilot design in the next generation wireless systems using deep learning.

ATHAR ALI MOINUDDIN (Member, IEEE) received the B.Sc., M.Sc., and Ph.D. degrees in electronics engineering from the Z. H. College of Engineering and Technology, AMU, Aligarh, India, in 1994, 1997, and 2010, respectively. During his Ph.D. work, he received the Commonwealth Split-Site Scholarship for one year (2007–2008) to conduct collaborative research at the Multimedia Networking Laboratory, University of Essex, UK. He has authored/coauthored 34 papers in refereed journals and conference proceedings of international repute. His research interests include low complexity image/video coding, standard image/video codecs, image/video communications, and wireless communications. He is a member of IAEng (Hong Kong) and IETE (India).